Supporting information for

Nanopores of Covalent Organic Framework- A Customizable Vessel for Organocatalysis

Debanjan Chakraborty,[ab] *Dinesh Mullangi,*[a] *Chandana Chandran,*[a] *and Ramanathan Vaidhyanathan*[ab*]

[a]Department of Chemistry, Indian Institute of Science Education and Research, Pune 411008, India.

[b]Centre for Energy Science, Indian Institute of Science Education and Research, Pune 411008, India.

Table of Content:

Table S1: Selected organic transformation catalyzed by metal-free COF…….S2-S10.

Table S2: Non-noble metal-based COF catalysts……..S11-S18.

Table S3: Noble-metal@COF as heterogeneous catalyst for organic transformations…….S19-S32.

References……..S32-S35.

Table S1: Selected organic transformation catalyzed by metal-free COF.

<table>
<tr><th>No.</th><th>Structure and Code of the COF and Notable properties</th><th>Catalysed Organic Reaction</th><th>Ref.</th></tr>
<tr><td colspan="4">Knoevenagel reaction</td></tr>
<tr><td>1</td><td> 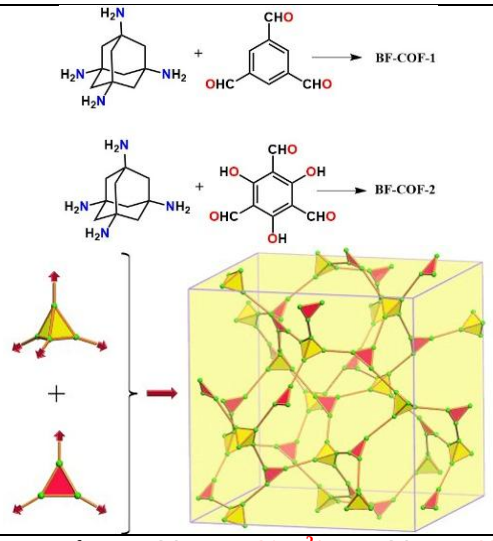
</td><td> 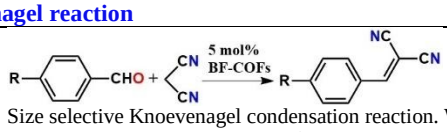

Size selective Knoevenagel condensation reaction. When R is H, the reaction yields >90 product. But if R= Me, Ph, Tol etc, the reaction doesn't proceed.
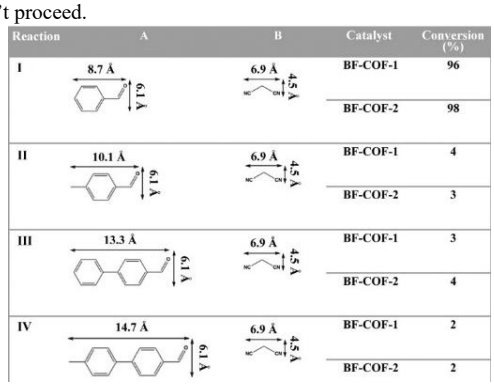
</td><td>S1</td></tr>
<tr><td colspan="4">BET Surface area for: BF-COF-1 = 730 m^2/g, BF-COF-2 = 680 m^2/g. Pore size from NLDFT fit: 8.3 Å for BF-COF-1 and 8.1 Å for BF-COF-2. Reprinted with the permission from the Wiley Online Library (reference S1).</td></tr>
<tr><td>2</td><td> 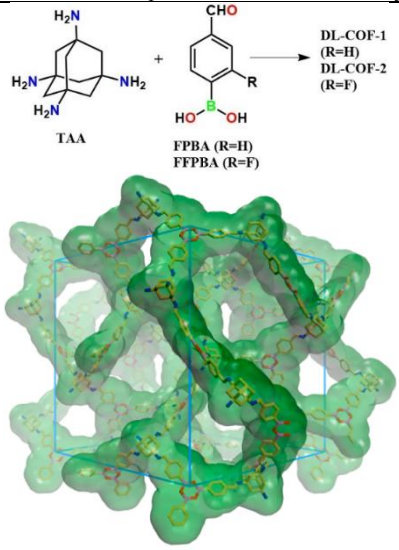

The 3- and 4-connected building units results in a 3D network with the cubic carbon nitride (ctn) topology,</td><td>One-Pot Cascade Reactions.
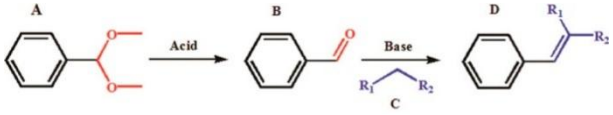

Step 1: Requires acidic sites, which are supplied by boroxine group
Step 2: Condensation step involves the basic sites from imine bonds in DL-COFs.
<table>
<tr><th>Entry</th><th>Catalyst</th><th>C</th><th>Conversion of D (%)</th></tr>
<tr><td>1</td><td>DL-COF-1</td><td>$R_1 = R_2 = CN$</td><td>98</td></tr>
<tr><td>2</td><td>DL-COF-2</td><td>$R_1 = R_2 = CN$</td><td>96</td></tr>
<tr><td>3</td><td>DL-COF-1</td><td>$R_1 = CN$, $R_2 = COOC_2H_5$</td><td>93</td></tr>
<tr><td>4</td><td>DL-COF-2</td><td>$R_1 = CN$, $R_2 = COOC_2H_5$</td><td>92</td></tr>
<tr><td>5</td><td>DL-COF-1</td><td>$R_1 = R_2 = COCH$</td><td>93</td></tr>
<tr><td>6</td><td>DL-COF-2</td><td>$R_1 = R_2 = COCH$</td><td>94</td></tr>
</table>
R_1: CN, COCH. R_2: CN, COCH, $COOC_2H_5$
Yield: 92-98%.</td><td>S2</td></tr>
<tr><td colspan="4">BET surface areas of DL-COF-1 and DL-COF-2 are 2259 and 2071 m^2/g. NLDFT pore sizes of DL-COF-1 and DL-COF-2 are 13.6 and 12.8 Å. H_2 uptake at 77K at 1 bar: 234 and 193 cc/g for DL-COF-1 and DL-COF-2. CO_2 uptake at 273K at 1 bar: 136 and 111 cc/g for DL-COF-1 and DL-COF-2. CH_4 uptake at 273K at 1 bar: 36 and 30 cc/g for DL-COF-1 and DL-COF-2 respectively. Reprinted with the permission from the American Chemical Society (reference S2).</td></tr>
<tr><td>3</td><td> 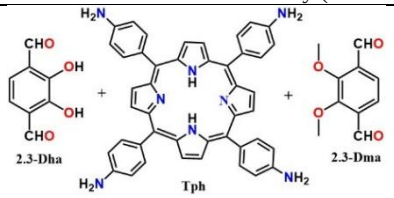
</td><td> 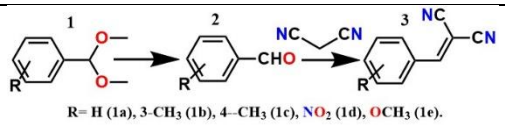
</td><td>S3</td></tr>
</table>

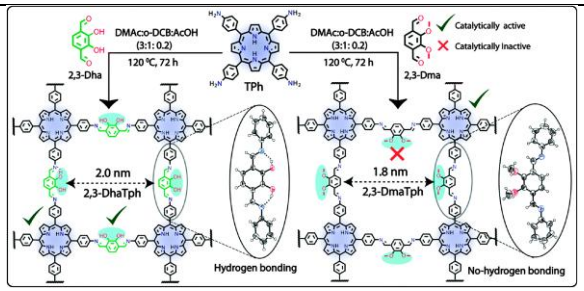

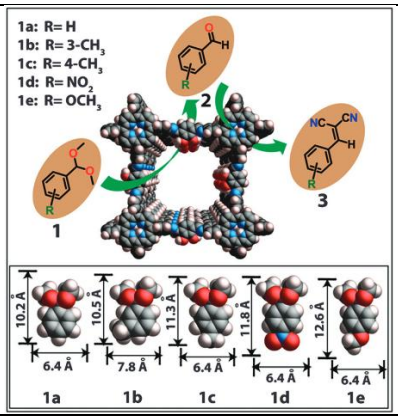

BET Surface areas of 2,3-DhaTph and 2,3-DmaTph are **1019** and **668 m^2/g**. NLDFT pore sizes are **2.2** and **1.4 nm**, respectively. Due to the presence of acidic (catechol) and basic (porphyrin) sites, 2,3-DhaTph shows significant selectivity, reusability, and excellent ability to perform the cascade reaction. Reprinted with the permission from the Royal Society of Chemistry (reference S3).

4

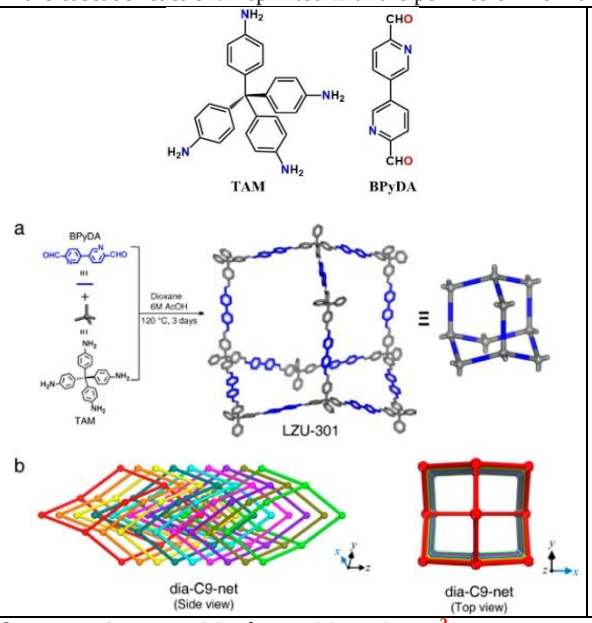

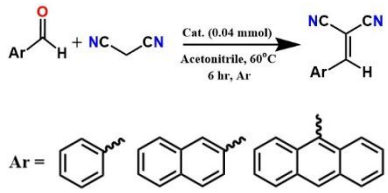

aldehyde	product	isolated yield for different catalysts (%) LZU-301	LZU-101	PyMA[b]	COF-320
1a	3a	72 (99)[c]	21	94	42
1b	3b	21	22	95	N/A
1c	3c	5	13	75	N/A
1a + 1c[d]	3a	~18[e]	N/A	N/A	N/A

[a]General conditions: aldehyde (1, 0.5 mmol), malononitrile (2, 1.5 mmol). [b]Reaction time: 4 h. [c]Prolong the reaction time to 10 h. [d]Ratio of 0.25 mmol vs 0.25 mmol. [e]GC yield.

S4

Notable properties: BET SA of LZU-301 is **654 m^2/g**; pore size: **5.8 × 10.4 Å^2** (contracted form) to **9.6 × 10.4 Å^2** (expanded form). Significant stepwise and hysteresis uptake is observed from THF adsorption isotherm at 283 K indicating LZU-301 retains its contracted phase for dynamic response at higher temperatures. Dynamic behaviour is studied by ^{129}Xe NMR spectroscopy. CO_2 uptakes are **2.63** and **1.59 mmol/g** at 273 and 298K respectively at 1 bar. Dynamic CO_2/N_2 separation at dry condition, 298K, 1 bar: CO_2 uptake is **0.22 mmol/g**. Uptake is **0.29 mmol/g** under **17% RH** and **0.37 mmol/g** under **83% RH** indicating water-assisted gate opening. Reprinted with the permission from the American Chemical Society (reference S4).

5

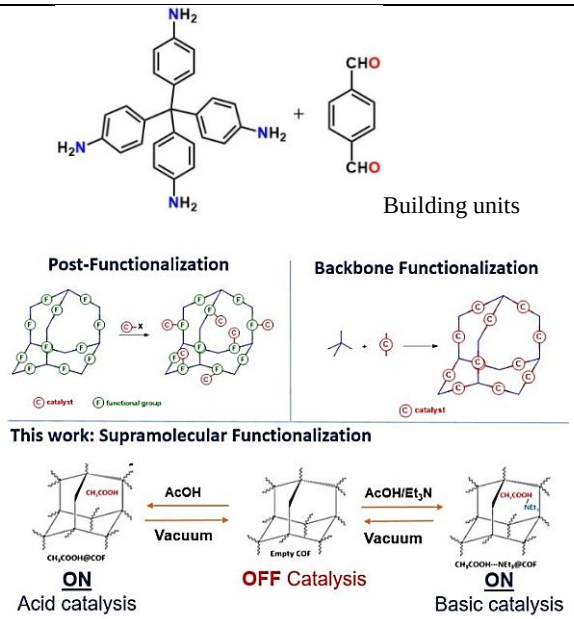

Strategies for the catalytic functionalization of materials and the supramolecular functionalization used in this work.

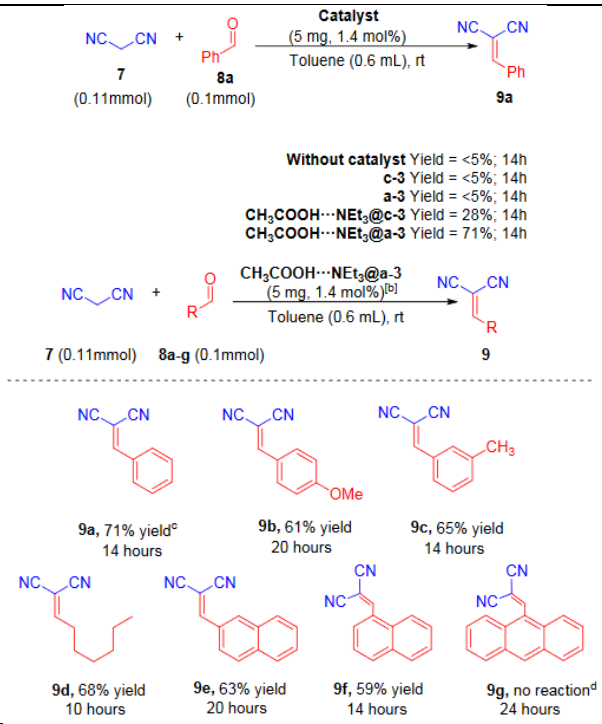

S5

COF-300 is modified with the acid (CH_3COOH) and base (NEt_3) to impose catalytic activity of ring-opening reaction of epoxides and the Knoevenagel reaction. The catalytic activity is modulated by confinement effect of the nano porous materials (supported by DFT studies) and this results in the size dependent catalytic activity. Energetics of the catalysis has been modeled. Reprinted with the permission from the Royal Society of Chmistry (reference S5).

CO_2 utilization

6

Synthesis of **IL-ADH**, **COF-IL** and its idealized structure.

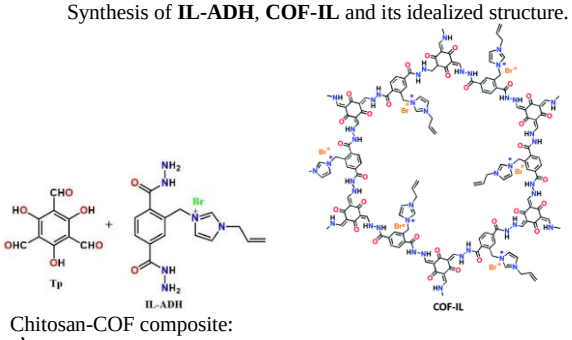

Chitosan-COF composite:

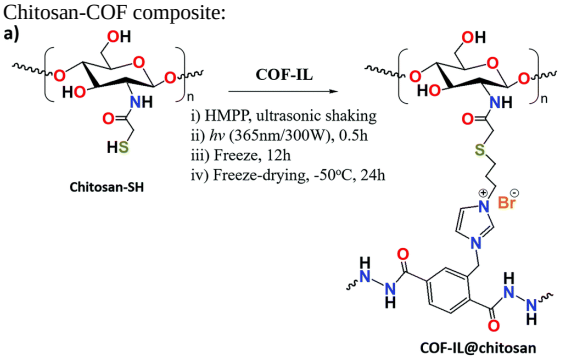

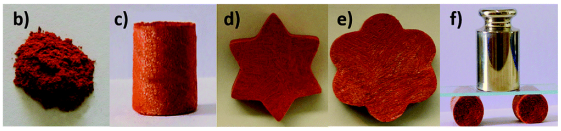

Fabrication of **COF-IL@chitosan** aerogel.

CO_2 cycloaddition with styrene oxide.

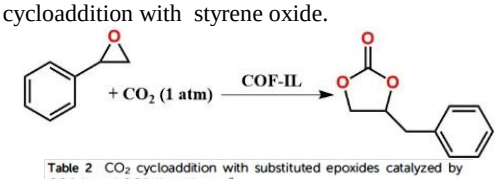

Table 2 CO_2 cycloaddition with substituted epoxides catalyzed by COF-IL and COF-IL@chitosan[a]

Entry	Substrate	COF-IL[b] (mol%)	T (°C)	t (h)	Yield[c] (%)
1		3.0	80	48	98
2		3.0	80	48	98
3		3.0	80	48	~100
4		3.0	80	48	97
5		3.0	80	48	89
6		3.0	80	48	71
7		3.0	80	48	7
8[d]		1.5	80	72	91

[a] Reaction conditions: 13.0 mmol of epoxide, 1 atm of CO_2, solvent-free, COF-IL. [b] Calculated based on the number of active sites in COF-IL. [c] Yields were determined by ^1H NMR spectra. [d] Scale-up experiment based on cuplike aerogel reactor: 175 mL (1.53 mol) of epoxy styrene, 1 atm of CO_2, 16.8 g of COF-IL@chitosan (1.5 mol% COF-IL equiv.), solvent-free.

S6

Ionic liquid decorated COF (COF-IL): BET SA: **291 m^2/g** and pore sizes are **16.5** and **22.2 Å**. CO_2 uptake: 106.04 cc/g@273K and 59.37k cc/g@298K at 1 bar. Zero loadig HOA: 28.8 kJ/mol. CO_2/N_2 selectivity: 43.38@273K and 59.96@298K. CO_2/CH_4 selectivity: 15.95@273K and 13.85@298K. CO_2/H_2 selectivity: 235.37@273K and 216.98@298K.
COF-IL@ chitosan: BET SA is **103.3 m^2/g**. CO_2 uptakes for the composite: 38.77 cc/g@273K and 25.83 cc/g@298K. Zero loading HOA is 16.3 kJ/mol. CO_2/N_2 selectivity: 93.65@273K and 98.82@298K. Reprinted with the permission from the royal Society of Chemistry (reference S6).

7

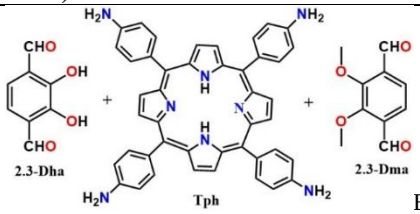

Building units

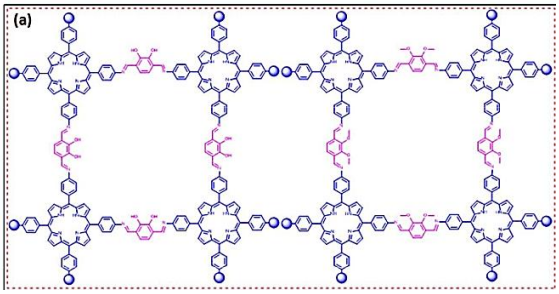

BET surface areas for for the COFs are ~**1000 m^2/g**.

CO_2 cycloaddition with epoxides:

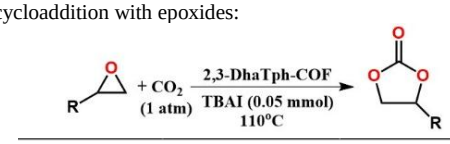

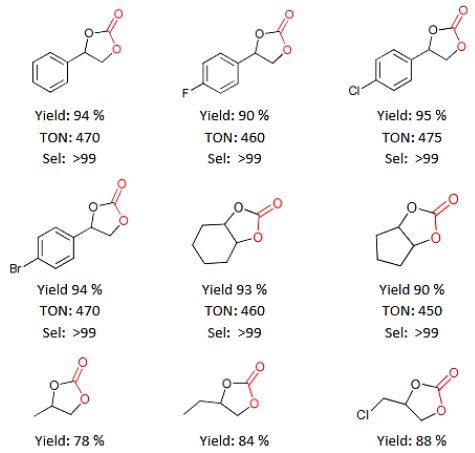

Synthesis of oxazolidinones:

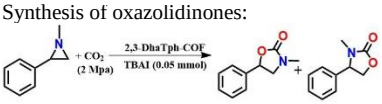

N-R, R: Me, Et, iPr, Benzyl, cyclohexyl etc. TON:195-480. Yield: 40-96%.
Reprinted with the permission from the Royal Society of Chemistry (reference S7).

S7

8

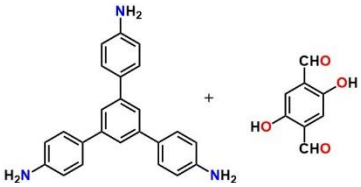

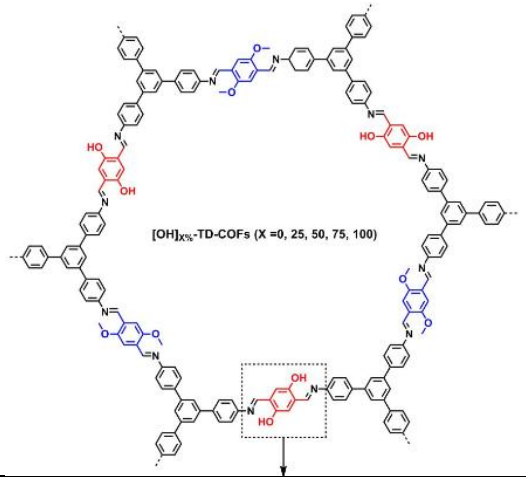

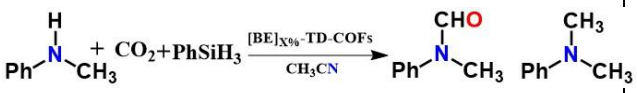

Reduction of CO_2 with N-methylaniline and $PhSiH_3$.

S8

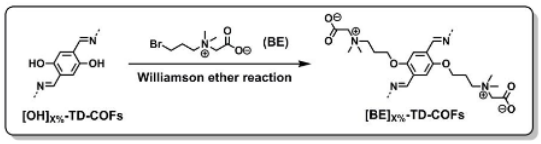

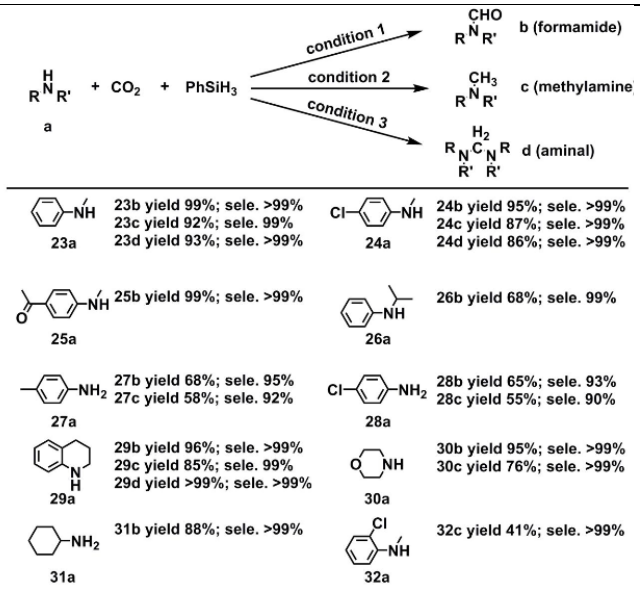

Zwitterionic COF, $[BE]_{X\%}$-TD-COFs: Betaine groups (BE) are introduced onto the channel walls of presynthesized frameworks via pore surface engineering methodology. BET SA and pore sizes vary with OH and BE's % loading. [OH] 0% to 100: **2280-1680 m^2/g** (**3.24 nm**). [BE] 0% to 75%: **2020-470 m^2/g** (**3.17-2.95 nm**). Reprinted with the permission from the American Chemical Society (reference S8).

9

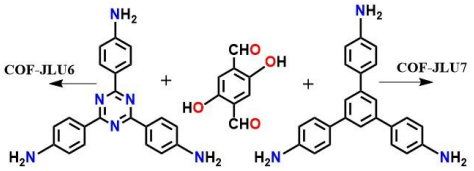

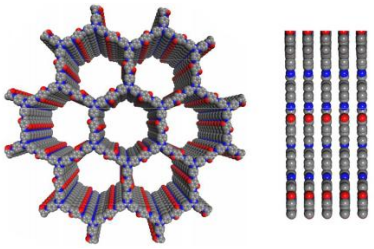

COF=JLU6

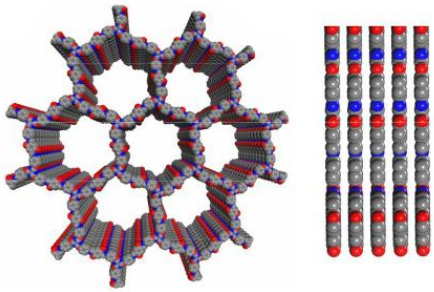

COF-JLU-7

Cycloaddition of CO_2 with epoxides to form cyclic carbonates.

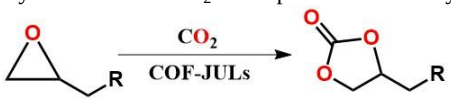

Entry	Substrate	Product	Yield (%)[b]
1		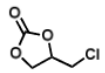	92 96[c]
2		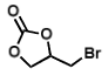	99 99[c]
3		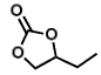	79 99[c]
4	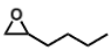	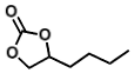	61 58[c]
5	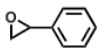	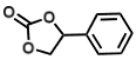	88[c]
6	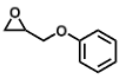	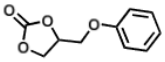	71[c]

[a]Reaction conditions: COF-JLU7 (0.051 mmol), epoxide (10.21 mmol), TBAB (0.51 mmol), CO_2 (0.1 MPa), 40 °C, and 48 h. [b]Determined by ^{1}H-NMR spectroscopic analysis.[c]80 °C and 12 h.

S9

BET surface areas for COF-JLU6 and COF-JLU7 are **1450** and **1392 m^2/g**. Pore sizes are **3.3** and **3.4 nm** for COF-JLU6 and COF-JLU7. CO_2 uptakes are 129 and 151 mg/g for COF-JLU6 and COF-JLU7 respectively at 273K, 1 bar. Zero loading HOAs are 30.8 and 28.1 kJ/mol for COF-JLU6 and COF-JLU7. Reprinted with the permission from the Royal Society of Chemistry (reference S9).

Biomimetic-catalysis

10

S10

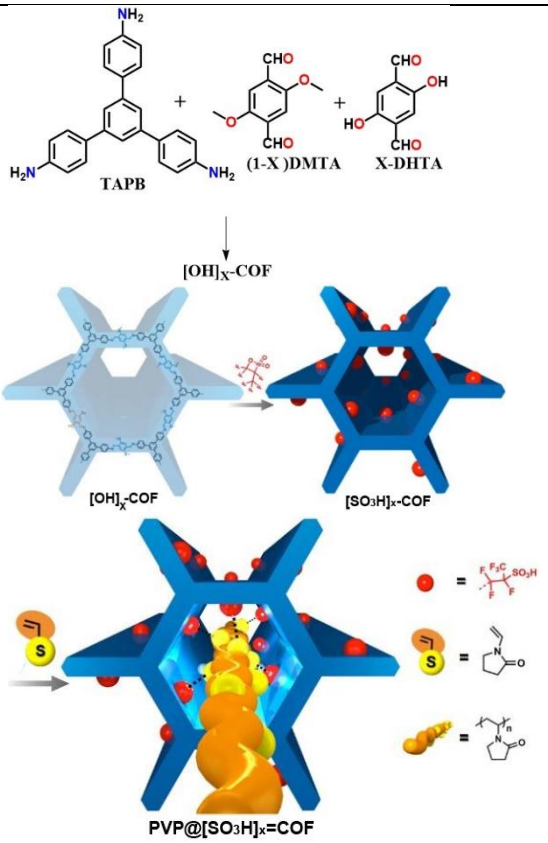

Synthesis scheme of PVP@[SO_3H]x-COF.

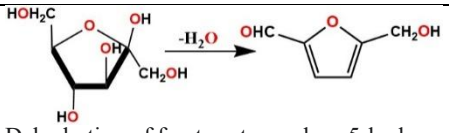

Dehydration of fructose to produce 5-hydroxymethylfurfural.

Entry	Catalyst	Time (min)	Conv. (%)	Select. (%) [b]	Yield (%) [b]
1 [c]	PVP@[SO_3H]$_{0.17}$-COF	30	>99.5	99.1	99.1
2	[SO_3H]$_{0.17}$-COF	30	23.2	77.1	17.9
		(120)	(94.6)	(35.2)	(33.3)
3	Nafion® NR50	30	9.7	54.6	5.3
		(360)	(89.3)	(19.4)	(17.3)
4	Amberlyst-15	30	15.3	67.1	10.3
		(180)	(95.2)	(29.5)	(28.1)
5	TsOH	30	28.5	73.5	20.9
		(120)	(>99.5)	(37.8)	(37.8)
6	PVP&DVB@[SO_3H]$_{0.17}$-COF	30	86.7	62.7	54.9
7	PVP@[SO_3H]$_{0.33}$-COF	30	96.4	89.3	86.1
8	PVP@[SO_3H]$_{0.50}$-COF	30	91.2	75.6	68.9
9 [d]	PVP@[SO_3H]$_{0.17}$-COF	30	>99.5	97.1	97.1
10 [e]	PVP@[SO_3H]$_{0.17}$-COF	30	>99.5	98.2	98.2

[a] Reaction conditions: fructose (100 mg, 0.56 mmol), catalyst (based on the amount of sulfonic acid 2.0 mol%), 100 °C, THF (3.0 mL), and the reaction time has been optimized; [b] the HMF selectivity and yield were determined by the combination of liquid chromatography and gas chromatography. [c] isolated HMF yield 94.5% (Figure S12). [d] recycle for 5 times. [e] fructose (1.0 g), PVP@[SO_3H]$_{0.17}$-COF (2.0 mol%), 100 °C, and THF (20 mL) for 30 min; The values in parentheses refer to the time used, as well as the conversion of fructose and selectivity and yield of HMF at that point.

BET SA: [OH]$_{0.17}$-COF: **1898 m^2/g**. [SO_3H]$_{0.17}$-COF: **1510 m^2/g** (pore size = **3.3 nm**). PVP@[SO_3H]$_{0.17}$-COF: **644 m^2/g**. Reprinted with the permission from the Wiley Online Library (reference S10).

11

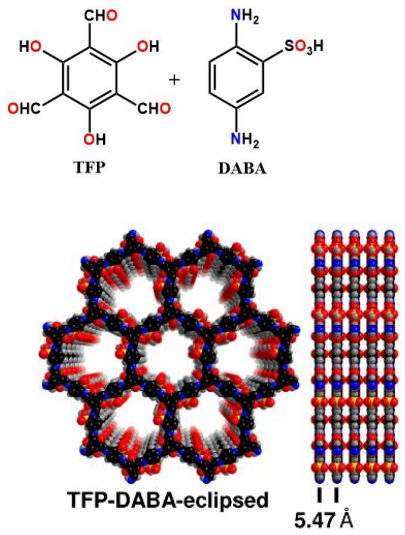

Synthesis of 5-hydroxymethylfurfural from fructose using TFP-DABA.

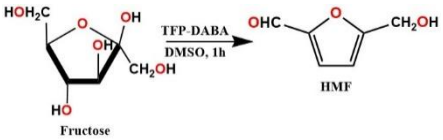

Yield: > 90% for HMF.

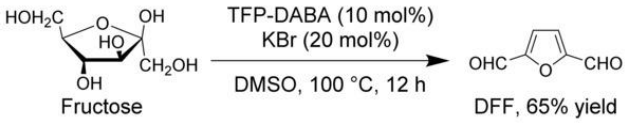

One-pot synthesis of DFF from fructose catalyzed by TFP-DABA and KBr. Yield 65%.

S11

The amount of dangling sulfonic acid groups in TFP-DABA is estimated to be **3.15 mmol/g** by acid–base titration, which is comparable to the theoretical value of 3.42mmol/g. BET SA is **158 m^2/g** and the pore size is **1.4 nm**. Reprinted with the permission from the Wiley Online Library (reference S11).

Epoxidation Reaction

12

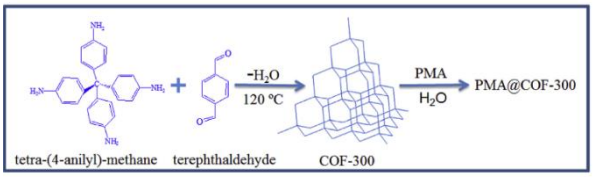

12-phosphomolybdic acid (PMA) immobilized in the COF.
Preparation conditions and doping levels of catalysts.

Catalyst	Temp. (°C)	Mo (%)	PMA (mmol/g)
PMA@COF-300a	20	4.13	0.04
PMA@COF-300b	80	4.22	0.04
PMA@COF-300c	80	16.22	0.14

Olefin epoxidation.

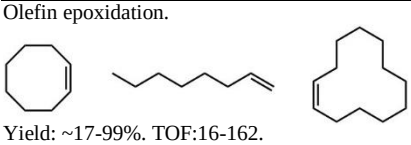

Yield: ~17-99%. TOF:16-162.

(i) High selectivity of epoxycyclooctane in 3 h at 50 °C.
(ii) Notably, the relatively inert terminal alkene of 1-octene can also be converted to epoxide at a reaction temperature of 60 °C.
(iii) It was found that this relatively bulky cyclododecene (with kinetic diameter of around 8 Å) could also be converted to corresponding epoxide over the PMA supported catalysts.

Reprinted with the permission from the Elsevier (reference S12).

S12

Michael addition and Diels-Alder reaction

13

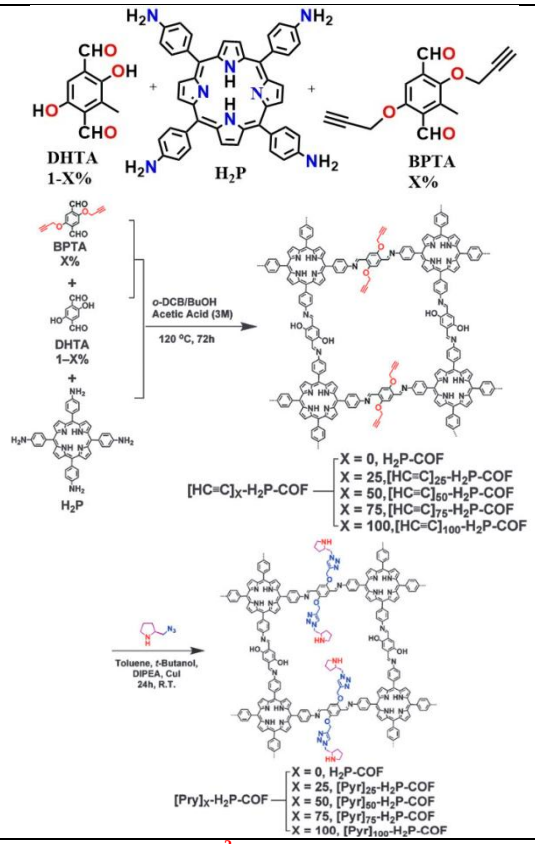

Michael addition reaction

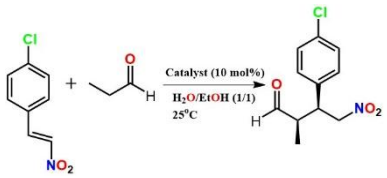

	Time for 100% conversion (h)	dr	ee (%)
Control	3.3	60/40	49
$[Pyr]_{25}$-H_2P-COF	1	70/30	49
$[Pyr]_{50}$-H_2P-COF	2.5	70/30	50
$[Pyr]_{75}$-H_2P-COF	5	70/30	51
$[Pyr]_{100}$-H_2P-COF	9	65/35	44

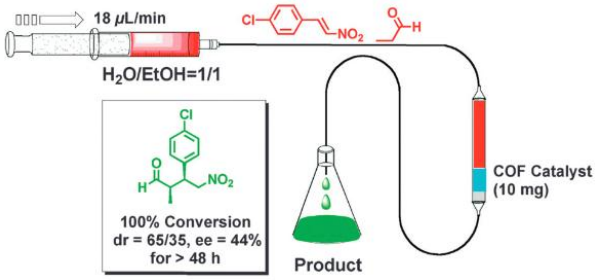

Flow reaction system for the organocatalytic COF column.

S13

BET SA of COF-SQ is **1195 m^2/g** and pore size is **3.6 nm**. Reprinted with the permission from the Royal Society of Chemistry (reference S13).

14

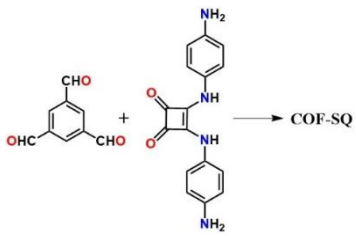

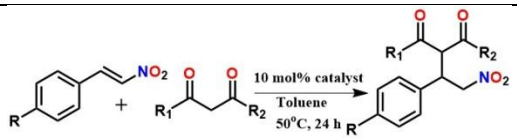

R: H, CH_3, OCH_3, Cl, Br. R1: H, CH_3. R2: H, OCH_3, OC_2H_5. Yield: 63-98%.

Michael addition reaction between b-nitrostyrene and 2,4-pentanedione[a]

S14

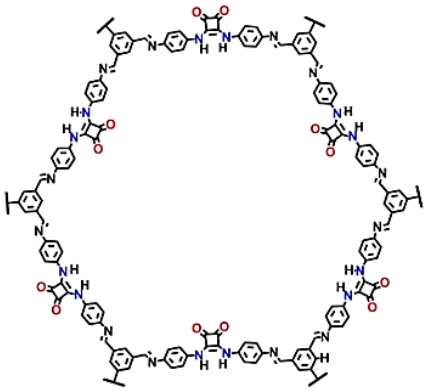

The framework provides efficient hydrogen bonding interaction leading to the catalysis.

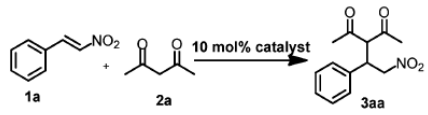

Entry	Catalyst	Temp (°C)	Time (h)	Solvent	Yield[b] (%)
1	**COF-SQ**	50	24	Toluene	95
2	**COF-SQ**	50	24	THF	70
3	**COF-SQ**	50	24	Acetone	40
4	**COF-SQ**	50	24	CH_2Cl_2	99
5	**COF-SQ**	50	24	$CHCl_3$	76
6	**COF-SQ**	50	24	DMSO	88
7	**COF-SQ**	50	24	MeOH	33
8	**COF-SQ**	50	24	CH_3CN	79
9	**COF-SQ**	r.t.	24	Toluene	75
10	**COF-SQ**	60	24	Toluene	98
11	**COF-SQ**[c]	50	24	Toluene	64
12	Monomer **1**	50	24	Toluene	35
13	Monomer **2**	50	24	Toluene	Trace
14	Model compound **4**	50	24	Toluene	63
15	**2DP$_{1+5}$**	50	24	Toluene	Trace

[a] Reaction condition: **1a** (0.10 mmol), **2a** (0.15 mmol), **COF-SQ** (10 mol%) in 1.0 mL solvent. [b] Determined by ^{1}H MNR spectroscopy of the crude mixture. [c] **COF-SQ** (5 mol%).

As the ethynyl content increases, $[HCRC]_X$-H_2P-COFs exhibit a decrease in the BET SA of **1126**, **1092**, **859**, **324**, and **206 m^2/g** as the ethynyl content increases from **0** to **25**, **50**, **75** and **100**, respectively, whereas their pore sizes decrease from **2.2** to **2.0**, **1.9**, **1.5**, and **1.5 nm**. The $[Pyr]_{25}$-H_2P-COF has a surface area of **960 m^2/g**, which decreases to **675**, **86**, and **63 m^2/g** for $[Pyr]_{50}$-H_2P-COF, $[Pyr]_{75}$-H_2P-COF, and $[Pyr]_{100}$-H_2P-COF, respectively. Their pore sizes decrease from **1.9** to **1.6**, **1.4**, and **1.4 nm**, respectively. Reprinted with the permission from the Royal Society of Chemistry (reference S14).

15

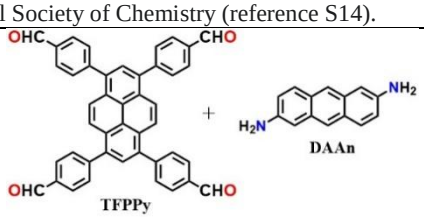

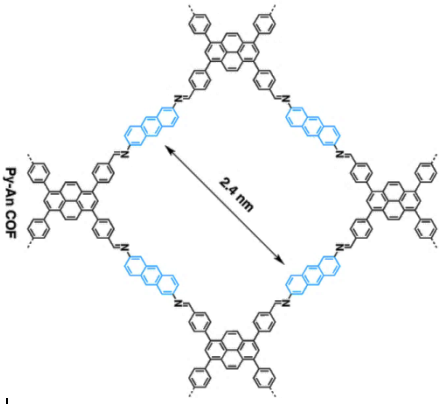

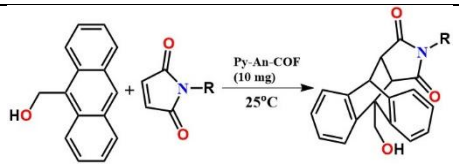

R: phenyl, benzyl, p-bromophenyl, p-nitrophenyl, cyclohexyl, ethyl. Yield: 60-90%.

Catalytic Diels-Alder reaction of 9-hydroxymethylanthracene and N-substituted maleimide using Py-An COF catalyst at 25C, 1bar.

Entry	R	Solvent	Reaction time (h)	Yield (%) No COF	Yield (%) With COF
1	Phenyl	EtOH	6	24	>99
2	Benzyl	EtOH	6	10	87
3	*p*-Bromophenyl	EtOH	24	21	83
4	*p*-Nitrophenyl	EtOH	24	5	50
5	Cyclohexyl	EtOH	24	22	60
6	Ethyl	EtOH	24	38	87
7	Phenyl	Water	48	13	91

S15

Py-An COF: BET SA is **1479 m^2/g** and pore size is **2.4 nm**. Pore volume = **0.7 cc/g**. Reprinted with the permission from the Royal Society of Chemistry (reference S15).

Phase-transfer Catalysis

16

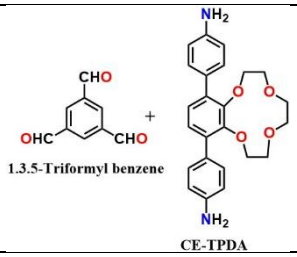

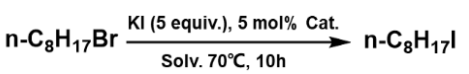

Phase Transfer Catalytic Activity of 18C6-COF in the Iodination of 1-bromooctane under Solid-Liquid-Solid Condition. When solvents are THF and EtOAc, yield = 96%.

Different nucleophilic substitution using different nucleophiles and the 18C6-COF as the phase transfer catalyst.

S16

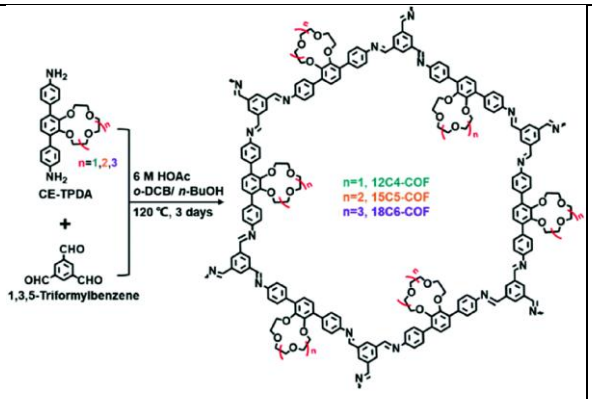

R-X + Nu^- —(10% mol 18C6-COF, Solv. reflux)→ RNu + X^-

Entry	RX	Nu^-	Solvent	T(℃)/t(h)	Yield (%)[b] /Controlled yield(%)[c]
1	n-C_4H_9Br	CH_3COOK	CH_3CN	85/5	85/27
2	n-$C_8H_{17}Br$	CH_3COOK	CH_3CN	85/5	91/26
3	$PhCH_2Br$	CH_3COOK	CH_3CN	85/5	99/34
4	$PhCH_2Cl$	CH_3COOK	CH_3CN	85/5	81/23
5[d]	$PhCH_2Br$	PhCOOK	NB/H_2O	100/10	96/25
6	$PhCH_2Br$	KSCN	CH_3CN	85 /1	99/31
7	$PhCH_2Br$	PhOK	CH_3CN	85/5	94/23
8	$PhCH_2Br$	NaN_3	CH_3CN	85/5	97/36
9	$PhCH_2Br$	KCN	CH_3CN	85/10	82/N.D. [e]
10	$PhCH_2Br$	KF	CH_3CN	85/10	84/N.D.
11		KF	CH_3CN	85/24	47/N.D.
12		KF	DMF	100/10	86/32

a Unless otherwise noted, the reaction conditions are: halides (0.25 mmol), nucleophile (1.25 mmol), and 18C6-COF (10 mol %, 14 mg), 2 mL solvent, GC-MS determined the structure. b GC yield. c Controlled experiment in the absence of catalyst. d 1.25 mmol PhCOOH + 1.5 mmol KOH in 1.5 mL H_2O and $PhCH_2Br$ in 0.5 mL nitrobenzene (NB). e N.D. = not detected the product.

Crown ether decorated COFs. BET surface areas of the 12C4-COF, 15C5-COF and18C6-COF are **210**, **59** and **47 m^2/g**. The pore size for the COFs are around **3.2 nm**. Reprinted with the permission from the Royal Society of Chemistry (reference S16).

Table S2: Non-noble metal-based COF catalysts.

<table>
<tr><th>No.</th><th>Structure and code of the COF and Notable properties</th><th>Catalysed Organic Reaction</th><th>Ref.</th></tr>
<tr><td colspan="4">Oxidation Reaction</td></tr>
<tr><td>1</td><td> 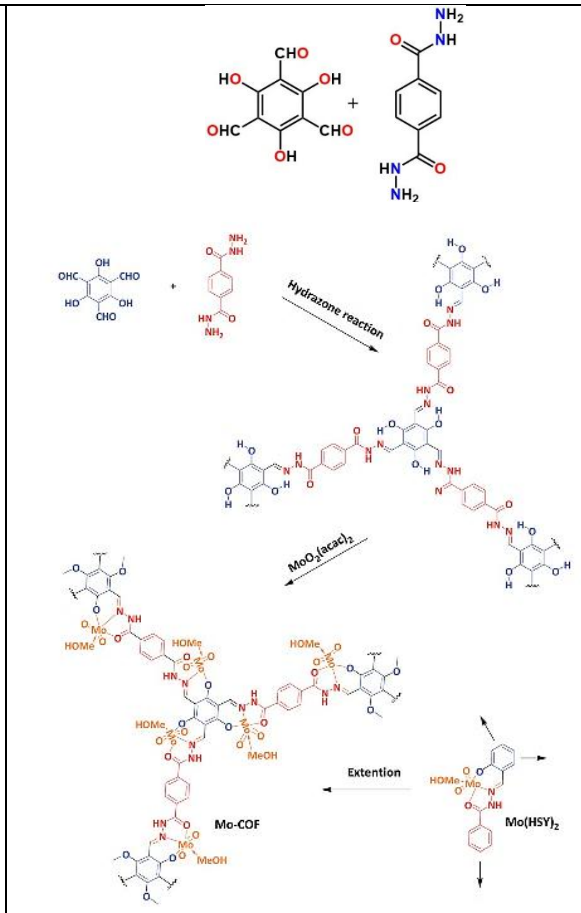
</td><td> 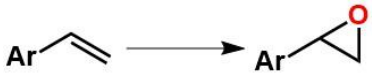
Epoxidation of alkenes.
Scope of the Mo-COF catalysed epoxidation of alkenes.[a]
<table>
<tr><th>Entry</th><th>Substrate</th><th>Product</th><th>Conversion[b]</th><th>Selectivity[c]</th></tr>
<tr><td>1</td><td></td><td></td><td>>99</td><td>71</td></tr>
<tr><td>2</td><td></td><td></td><td>80</td><td>>99</td></tr>
<tr><td>3</td><td></td><td></td><td>71</td><td>80</td></tr>
<tr><td>4</td><td></td><td></td><td>62</td><td>86</td></tr>
<tr><td>5</td><td></td><td></td><td>42</td><td>>99</td></tr>
<tr><td>6</td><td></td><td></td><td>20</td><td>>99</td></tr>
<tr><td>7</td><td></td><td></td><td>5</td><td>>99</td></tr>
</table>
[a]Olefin (1.0 mmol), TBHP (2.0 mmol), catalyst (0.01 mmol), 1,2-dichloroethane (2.0 mL) and bromobenzene (50 mg) as an internal standard sealed in a Teflon-lined screwcap vial were stirred at 80 C for 6h. [b] Conversion (%). [c] Selectivity (%) were determined by GC using an SE-54 column.</td><td>S17</td></tr>
<tr><td colspan="4">BET surface areas of COF and Mo-COF are 244 and 63 m^2/g. ICP-MS estimates the Mo contain to be 2 mmol/g. Active metal: Mo(VI). Reprinted with the permission from the Royal Society of Chemistry (reference S17).</td></tr>
<tr><td>2</td><td> 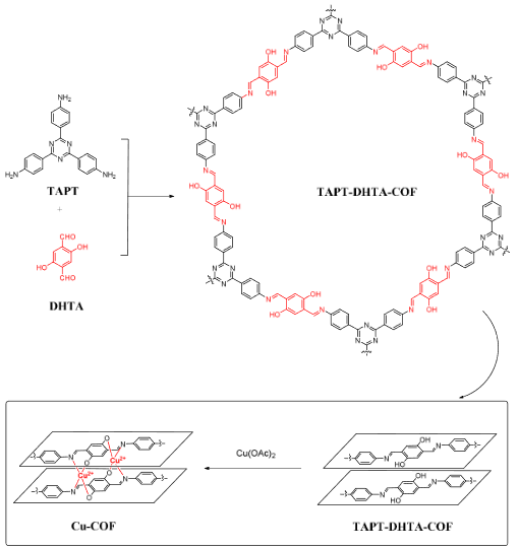
</td><td>Selective oxidation of styrene.
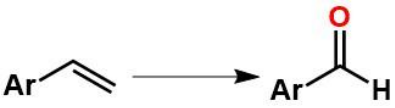 </td><td>S18</td></tr>
</table>

		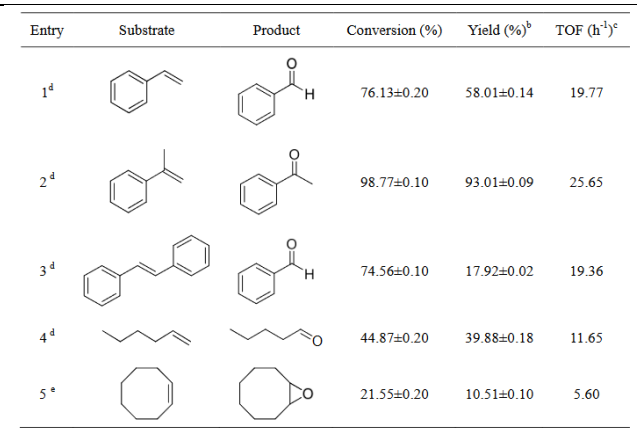	
Two methods are employed to synthesize the COF, reflux in DMF (TAPT-DHTA-COF_{DMF}) and solvothermal condition (TAPT-DHTA-COF_{HX}). The surface areas for the COF_{DMF} and COF_{HX} are **660** and **2238 m^2/g**. $Cu(OAc)_2$ is dissolved in methanol and then the COF is dispersed in the solution. The surface areas are reduced to **336** and **1886 m^2/g** for COF_{DMF} and COF_{HX} respectively. Active metal: **Cu(II)**. Reprinted with the permission from the American Chemical Society (reference S18).			
3	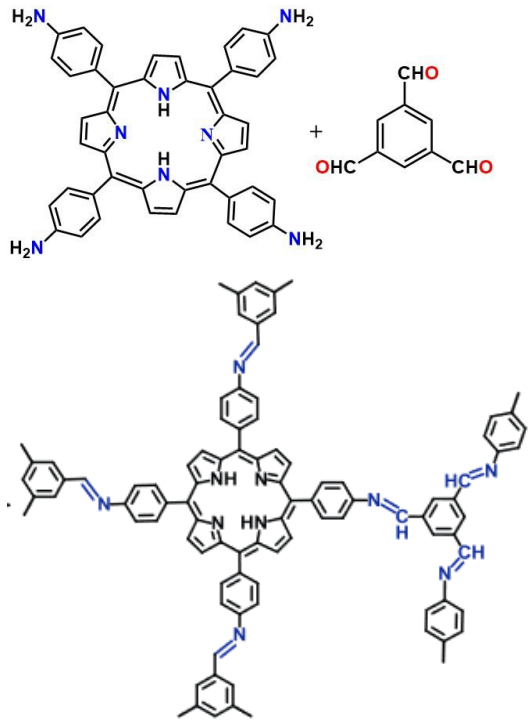	Selective aerobic epoxidation of olefins 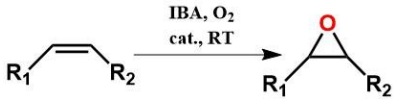 R1: Ph, cyclohexane, cyclopentane, cyclooctane etc. R2: H. RT, O_2 atm. 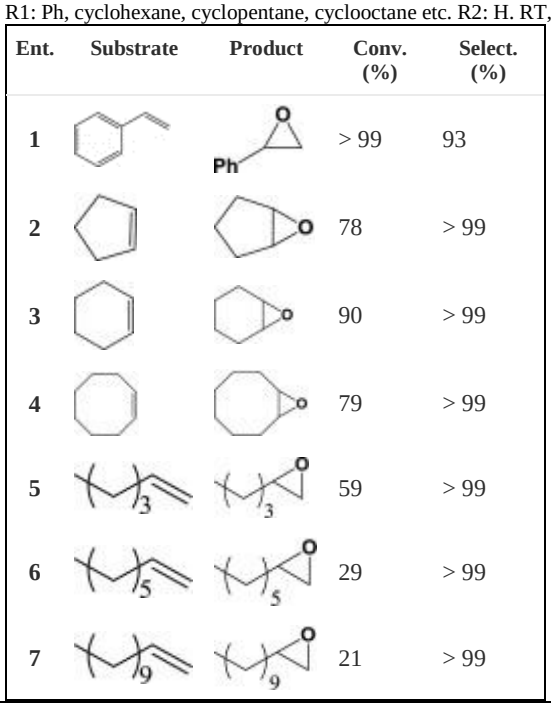	S19
The BET surface area of CPF-2 is **660 m^2/g** and pore size are **1.55 nm**. The BET surface areas of Co-CPF-2 and Mn-CPF-2 are **475** and **454 m^2/g**. ICP-MS: Co-CPF-2 and Mn-CPF-2 contain **4.71 Co** and **4.03 wt%** Mn ions, respectively. Active species: **Co(II)** and **Mn(II)**. Reprinted with the permission from the Elsevier (reference S19).			
4	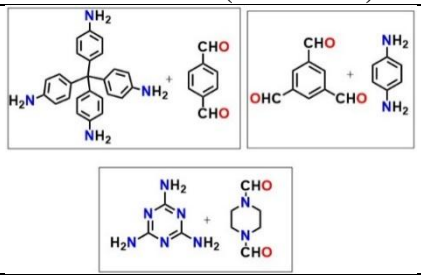	Epoxidation ofcyclooctene with H_2O_2: 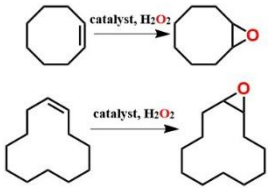	S20

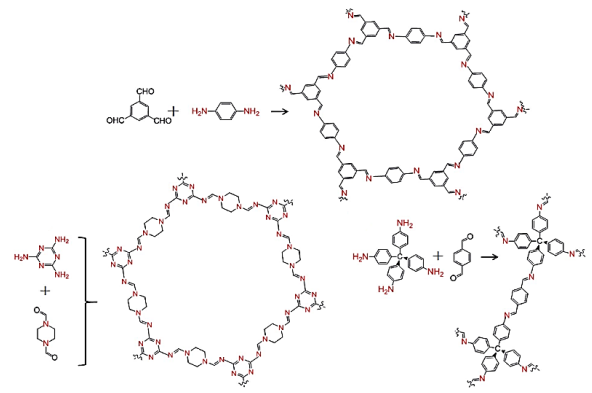

Substrate	Catalyst	Con. (%)	Selectivity (%)
	PMA@COF-LZU1	49	≥99
	Fe/PMA@COF-LZU1	69	
	PMA@CIN-1	83	
	Fe/PMA@CIN-1	88	
	PMA@COF-300	52	
	Fe/PMA@COF-300	62	
	Fe/PMA@CIN-1	58	≥99

Note: The COF and the COF-composites s do not exhibit high degree of crystallinity.

Fe-doped $H_3PMo_{12}O_{40}$ immobilized on covalentorganic frameworks (Fe/PMA@COFs). BET SA: COF-LZU1: **207 m^2/g**, Fe/PMA@ COF-LZU1: **35 m^2/g**, CIN-1: **246 m^2/g**, Fe/PMA@CIN-1: **77 m^2/g**, COF-300: **284 m^2/g**, Fe/PMA@COF-300: **56 m^2/g**. Active species: **Fe^{3+}** and **PMo_{12}^{3-}**. Reprinted with the permission from the Royal Society of Chemistry (reference S20).

5

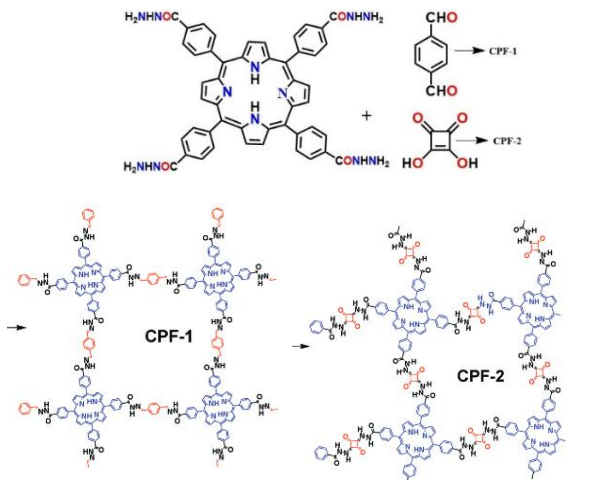

Mn–CPF-catalysed epoxidation of alkenes.

Scope of Mn-CPF-catalysed epoxidation of alkenes[a]

Entry	Substrate	Product	Catalyst	Conversion[b]	Selectivity[c]
1			Mn–CPF-1	99/96[d]	68/62[e]
2			Mn–CPF-2	93	60
3			Mn–CPF-1	99	>99
4			Mn–CPF-1	95	>99
5			Mn–CPF-1	81	>99
6			Mn–CPF-1	66	>99
7	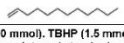	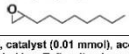	Mn–CPF-1	20	>99

[a]Olefin (1.0 mmol), TBHP (1.5 mmol), catalyst (0.01 mmol), acetonitrile (3.0 mL) and bromobenzene (50 mg) as an internal standards sealed in a Teflon-lined screwcap vial were stirred at 80 C for 24h. [b]Conversion (%). [c]Selectivity (%) were determined by GC using an SE-54 column. 50 C for 1min, then 10 C per min upto 140 C and 140 C for 15min. [d]After thrid cycle. [e]The byproducts were benzaldehyde and benzeneacetaldehyde.

S21

BET SA for CPF-1 and CPF-2 are **158** and **92 m^2/g**. ICP-MS: Mn content of **1.7 mmol/g** for Mn-CPF-1 and **1.6 mmol/g** for Mn-CPF-2. Active metal: **Mn(II).** Reprinted with the permission from the Royal Society of Chemistry (reference S21).

Glaser-Hay Coupling

6

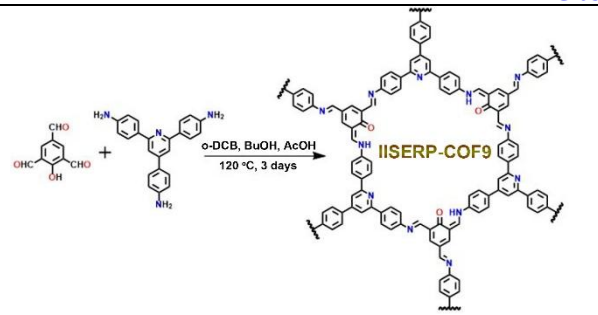

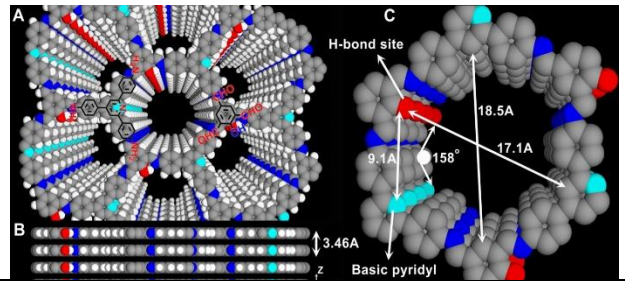

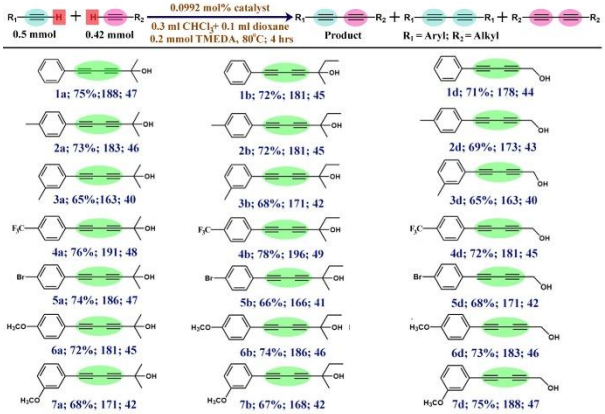

High selectivity for heteroproducts governed by substrate binding and orientation directed by the COF nanopore.

S22

	Periodic lining of the channels by the hydrogen-bonding hydroxyl and basic pyridyl sites (shown in cyan) and the channel dimensions.	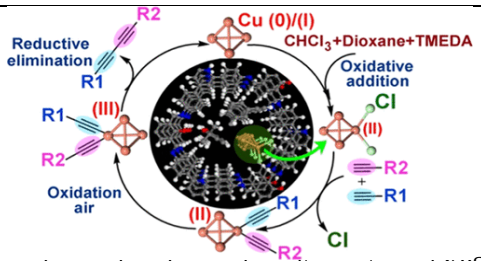 Reaction mechanism based on cyclic voltammetry and XPS done on frozen reactions. Labile Cl and variable oxidations on Cu are crucial.	
BET SA: **1171 m^2/g** and pore size **13 Å**. Cu content ~**5 wt%**. Active metal is **Cu(0)/Cu(I)**. Reprinted with the permission from the American Chemical Society (reference S22).			
Chan–Lamcoupling			
7	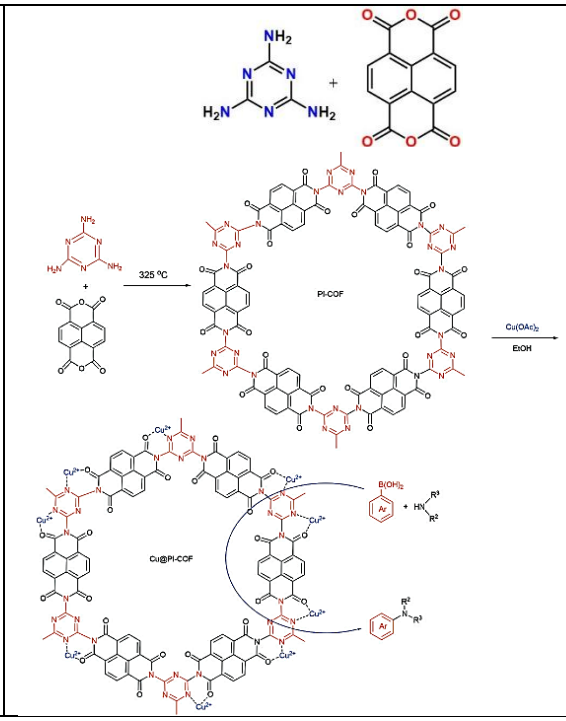	Chan–Lamcoupling reaction of aryl boronic acids andamines. 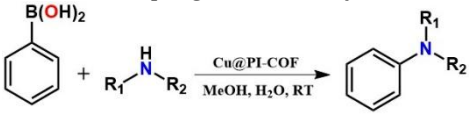 R_1 and R_2 are different aliphatic and aromatic groups. Yield: >80% 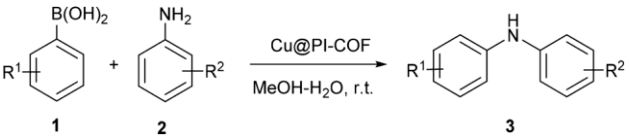 *N*-arylation of 1*H*-indazol-3-amine has also been investigated. For all three reactions several electron withdrawing and donating substrate scope has been investigated.	S23
The structure has not been modeled and the PXRD does not suggest a typical COF structure. No porosity has been reported. ICP-MS: Cu loading **5.33 wt%**. Active species: **Cu(II)**. Reprinted with the permission from the Royal Society of Chemistry (reference S23).			
Prins Reaction and Mannich-Type Reaction			
8	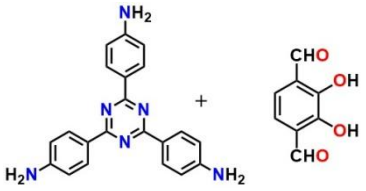	Prins condensation: 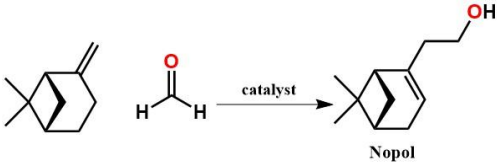 Yield >90%.	S24

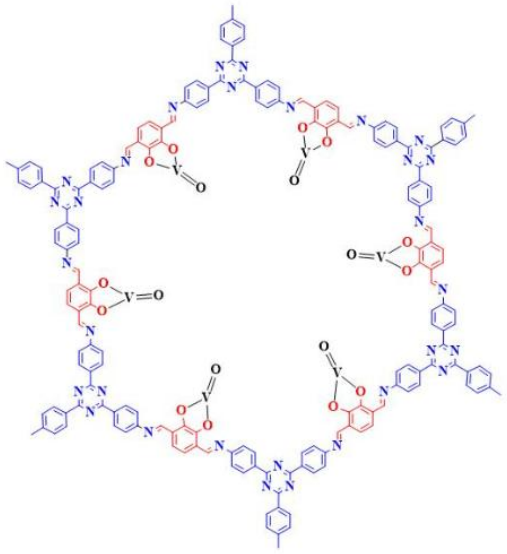

VO-TAPT-2,3-DHTA COF

Existense of V4+ is supported by XPS and EPR spectra.

Sulfide Oxidation with Differently Substituted Substrates Catalyzed with VO–TAPT–2,3-DHTA COF and Other Homogenous Analogue[a]

Entry	Sulphide	Sulphoxide	Time (h)	Conver. %	Yield %
1			4	99	96
2			4	99	95
3[b]			4	84	75
4[c]			4	93	81
5			4	96	92
6			4	97	93
7	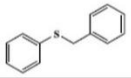	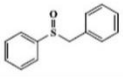	4	88	82

[a]Reaction condition: Sulfide (1.0 mmol). TBHP (1.5 mmol), catalyst (20mg) containing 0.019 mmol of vandadium; CH3CN (3ml.); 25 C; 100rpm; 4h. [b]Reaction was carried out using VO(acac)2 (4mol%); [c]using VO(catehol)2 (4mol%)

BET SA of TAPT-2,3-DHTA and VO- TAPT-2,3-DHTA are **1151** and **562 m^2/g**. Pore sizes are **3** and **2.5 nm**, respectively. Active metal: **V(V).** Reprinted with the permission from the American Chemical Society (reference S24).

9

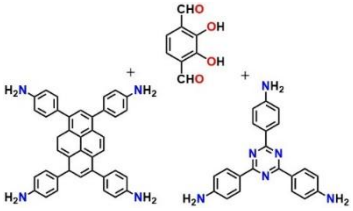

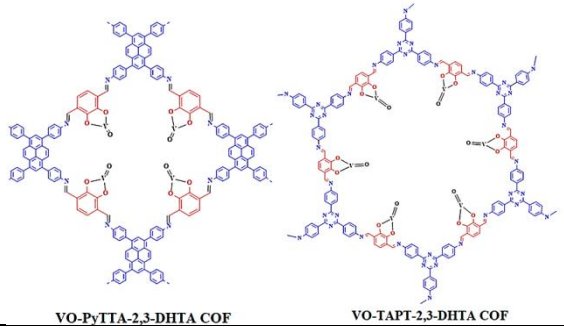

VO-PyTTA-2,3-DHTA COF **VO-TAPT-2,3-DHTA COF**

Mannich-Type Reaction

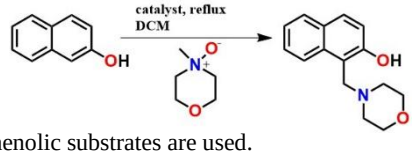

Different phenolic substrates are used.
Yield >90 %.
Proposed mechanism:

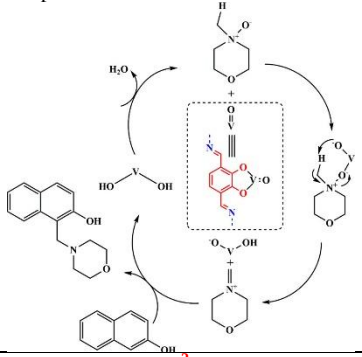

S25

BET surface area and pore size: TAPT-2,3-DHTA and PyTTA-2,3-DHTA COFs are **1151 m^2/g**, **3.0 nm** and **1892 m^2/g**, **1.6 nm**, respectively. CO_2 capacities of the TAPT-2,3-DHTA and PyTTA-2,3-DHTA COFs are 38 cc/g and 35 cc/g at 298K at 1 bar. BET SA and pore sizes of V doped COFs: VO-TAPT-2,3-DHTA and VO-PyTTA-2,3-DHTA are **562 m^2/g**, **2.5 nm** and **1382 m^2/g**, **1.5 nm**, respectively. Active metal: **V(V).** Reprinted with the permission from the American Chemical Society (reference S25).

Cross Coupling reaction

10 Decarboxylative cross-coupling reaction: S26

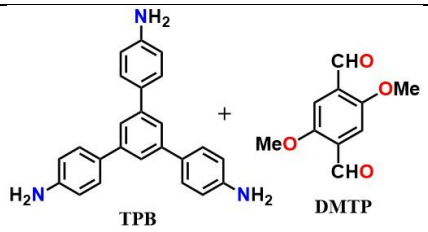

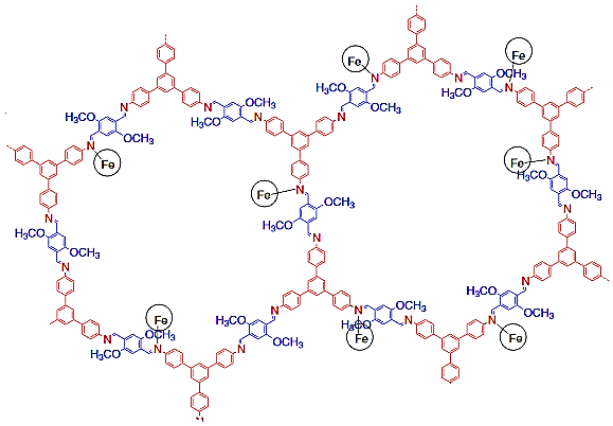

The COF loses crystallinity upon loading of $FeCl_3$ under THF at 70°C. And the porosity drops as reflected by the lowered surface area. But the isotherm profile remains the same (Type IV).
A loading of 1.07 mol of Fe^{3+} per TBP moiety translating to 3 Fe^{3+} per cage is estimated.

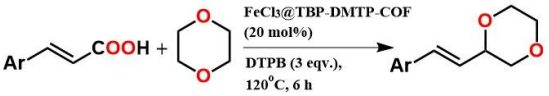

Ar: 4-Cl, 4-OH, 4-CH_3, 2-CH_3, 4-OCH_3, 2-OCH_3 substituted phenyl groups.

Entry	Ar	Yield (%)[a]
1	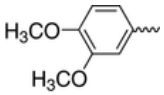	79
2	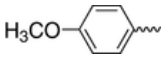	71
3[b]	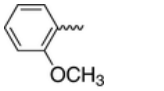	47
4[c]	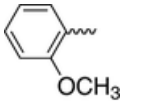	42
5	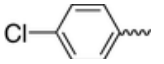	62
6	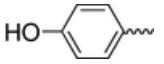	69
7	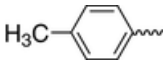	73
8	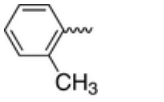	28

Reaction conditions, unless otherwise specified: cinnamic acid (0.067 mmol), 1,4-dioxane (0.5 mL), DTBP (3.0 equivalent), $FeCl_3$@TPB-DMTP-COF (20 mmol%), 6 h, 120 °C; [a]Isolated yields; [b]*E* isomer of the cinnamic acid was used; [c]*Z* isomer of the cinnamic acid was used.

BET SA of TPB-DMTP-COF and $FeCl_3$@TPB-DMTP-COF are **1200** and **235 m^2/g**. Pore size: **34.3 Å** for TPB-DMTP-COF and **31.4 Å** for $FeCl_3$@ TPB-DMTP-COF. AAS: Fe^{3+} loading = **7.85 wt%**. Active metal: **Fe(III)**. Reprinted with the permission from the Springer (reference S26).

Suzuki- Miyaura Coulpling

11

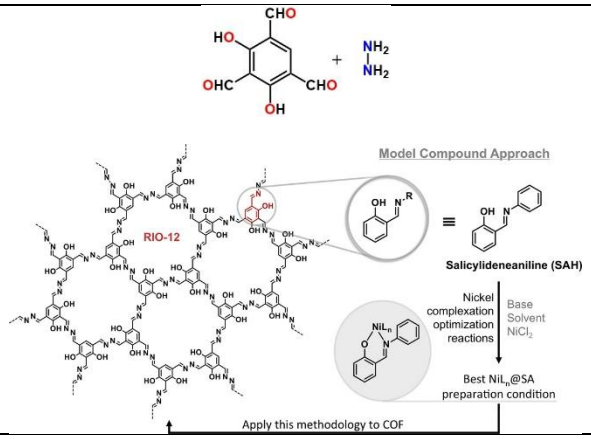

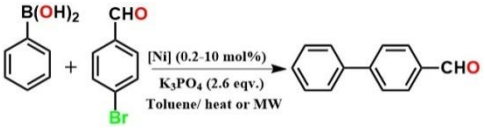

Suzuki-Miyaura cross-coupling reaction catalysed by Ni(II) doped COF. The reaction is done under microwave condition. No activity under conventional reflux conditions. Extreme care has been taken to keep the reactions dry and in a glove box.

Yield: 0 to 34% (only under Microwave conditions)

Note: Interestingly, no Ni^{2+} leaching was found, but the activity is only moderate and the conversion drops every cycle. This

S27

	The Ni^{2+} binding site of the COF resembles simple salicylidene type unit, well known to bind to Ni^{2+}.	suggests that even as well dispersed sites anchored on COF, the catalytic activity can be lost over cycles.	
BET SA of RIO-12 is **1458 m^2/g**. Pore is **17 Å**. ICP-AES: Ni^{2+} loading = **3.6 to 25 wt %**. Active species: **Ni(II).** Reprinted with the Wiley Online Library (reference S27).			
Reductive Cleavage of C-S bond or Desulfurization, Nitro/Nitrile reduction reaction			
12	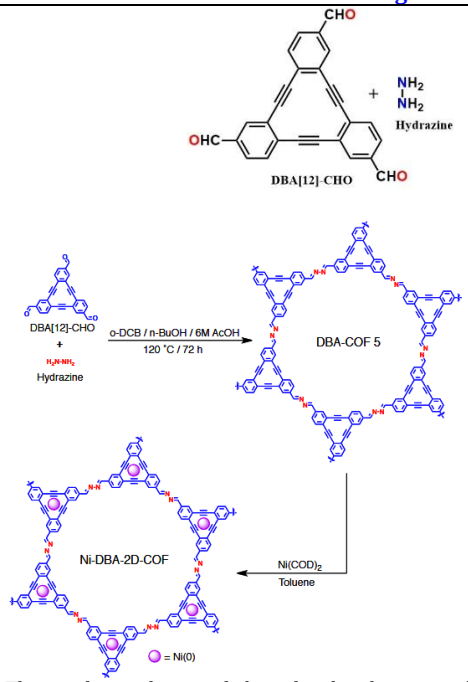 The metal is predominantly bound within the cavity of DBA[12] to produce a Ni(0) 16-electron complex with virtually no interaction at the azine linkage. Hence, the Nickel loading does not alter the surface area substantially.	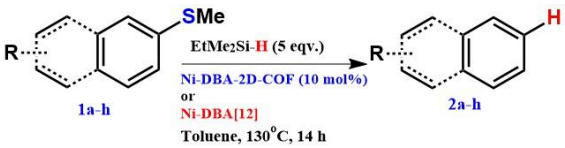 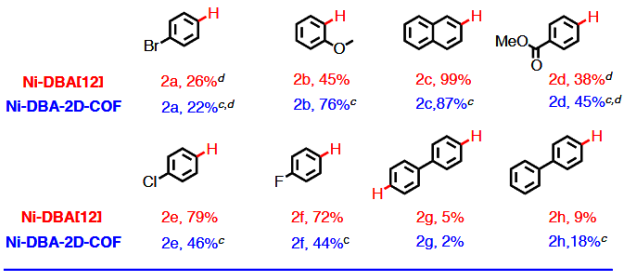 Reductive cleavage of aryl C-S bonds. The DFT calculations suggest that the Ni has to pop out of the DBA[12] cavity and bind with only one alkynyl unit to form a three-coordinate complex before it can oxidatively add into the C(aryl)–SMe bond. Such metal(0) popping out is known in Pd(0) catalysis. This is one of the rare cases, where a first-row transition metal has been suggested to do that.	S28
BET SA: for the DBA-COF 5 and Ni-DBA-2D-COF are **1643** and **1565 m^2/g,** respectively. The pore sizes are **1.9** and **1.8 nm**, while pore volumes are **0.70** and **0.68 cc/g** for DBA-COF 5 and Ni-DBA-2D-COF respectively (at P/P_0 0.899). ICP-AES found **8.56 wt%** of Ni. Active metal: **Ni(0)**. Reprinted with the permission from the American Chemical Society (reference S28).			

13

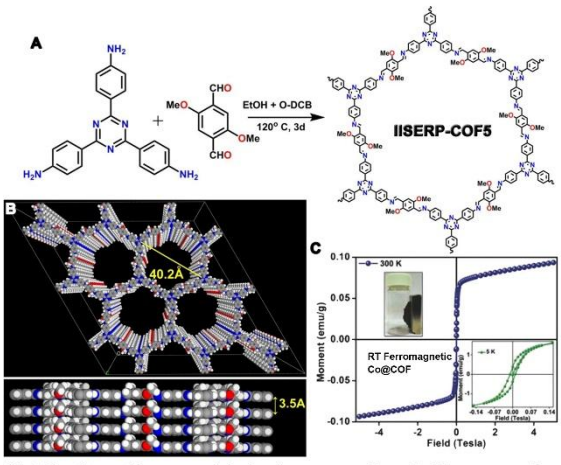

Stabilization of large metal-clusters exceeding limiting pore-size

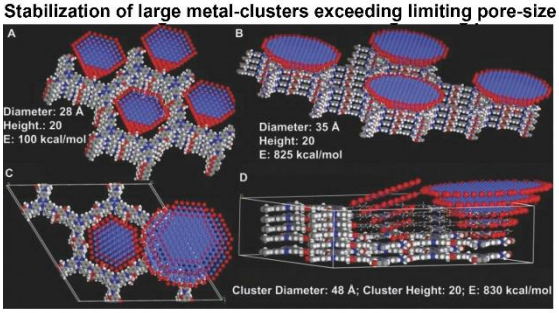

Ferromagnetic Co@COF. Methoxy fucntionalities renders high chemical stability.

S29

Reduction of nitrile to primary amine

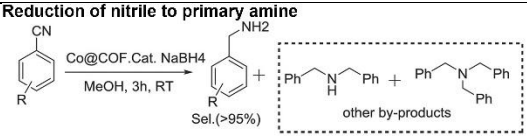

Activation of BH_4^- at the Cobalt facets- rapid H_2 release & reduction

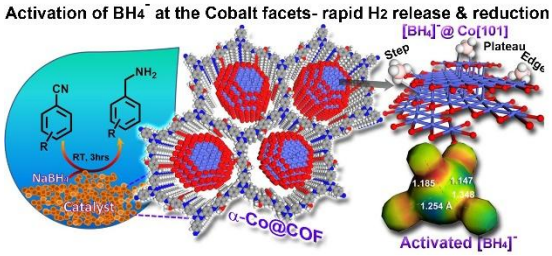

Co@COF catalysed H_2 evolution from NaBH4 in < 2min at RT

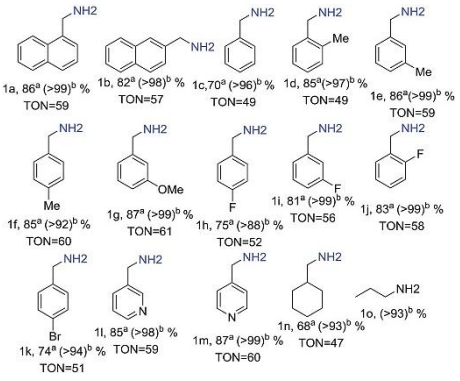

BET SA: IISERP-COF5 = **1036 m^2 g^{-1}**. BJH model: Pore size **≈36 Å** and pore volume of **1.154 cc g^{-1}**. Co nP loading: **18 wt%**. Co nP size = **3-5 nm**. Active species: **Co(0) and Co(II)** (from surface $Co(OH)_2$). Reprinted with the permission from the Wiley Online Library (reference S29).

Cyanosilylation of aldehydes

14

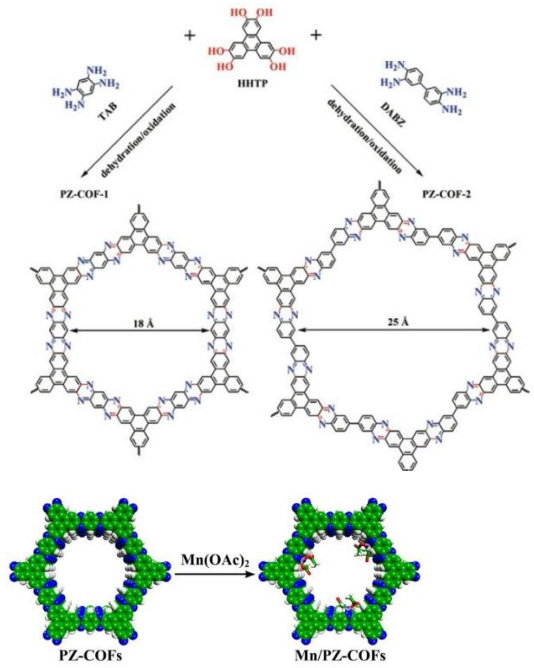

S30

Cyanosilylation of aldehydes:

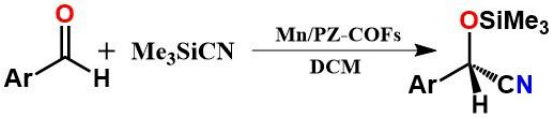

Ar: Phenyl, biphenyl, 1-napthyl, methoxyphenyl etc.

Entry	Ar	Catalyst	Time (h)	Yield[b] (%)
1	Phenyl	Mn/PZ-COF-1	6	98
2	Phenyl	Mn/PZ-COF-2	5	99
3	Biphenyl	Mn/PZ-COF-1	6	97
4	Biphenyl	Mn/PZ-COF-2	5	97
5	1-Naphthyl	Mn/PZ-COF-1	6	96
6	1-Naphthyl	Mn/PZ-COF-2	5	97
7	Methoxyphenyl	Mn/PZ-COF-1	8	97
8	Methoxyphenyl	Mn/PZ-COF-2	8	98
9	Nitrophenyl	Mn/PZ-COF-1	3	96
10	Nitrophenyl	Mn/PZ-COF-2	3	98

[a] Reaction conditions: Me_3SiCN (1.0 mmol), aldehyde (1.0 mmol), dry CH_2Cl_2 (6.0 mL), Mn/PZ-COF-1 or Mn/PZ-COF-2 (0.1 mmol), room temperature, under Ar. [b] Determined by ^1H NMR based on the starring materials.

Note: Despite well-defined cyclized imine-bond formation, these COFs do not exhibit high degree of crystallinity.

BET SA: PZ-COF-1: **845 m^2/g**, PZ-COF-2: **1130 m^2/g** and pore sizes **18** and **25 Å**. PZ-COF-1: 121 cc/g of H_2 at 77K, 68 cc/g of CO_2 at 273K, 14 cc/g of CH_4 at 273K. PZ-COF-2: 156 cc/g of H_2 at 77K, 91 cc/g of CO_2 at 273K, 21 cc/g of CH_4 at 273K. ICP: Mn loading was **6.3 wt%**. Active metal: **Mn(II).** Reprinted with the permission from the Royal Society of Chemistry (reference S30).

Table S3: Noble-metal@COF as heterogeneous catalyst for organic transformations.

<table>
<tr><th>Ent.</th><th>Structure and code of the COF and notable properties</th><th>Catalysed Organic Reaction</th><th>Ref.</th></tr>
<tr><td colspan="4">Bifunctional Catalysts using pre-designed pyridine groups in COF framework</td></tr>
<tr><td>1</td><td> 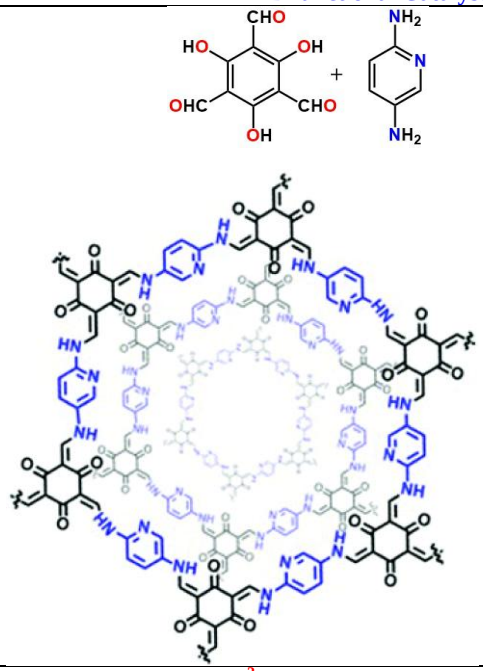
COF-TpPa-Py: BET SA 1019 m^2/g and pore size is 1.5 nm. ICP: Pd loading in Pd/COF-TpPa-Py = 4.1 and in Pd/POP-Py = 3.9 wt%. Active species: Pd(0). Reprinted with the permission from the Royal Society of Chemistry (reference S31).</td><td> 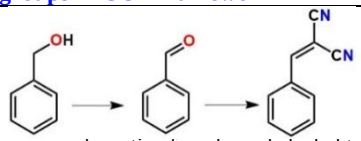
Cascade oxidation-Knoevenagel reaction from benzyl alcohol to benzylidene malononitrile. Yield: 98% of benzylidene malonitrile.
Pd/COF-TpPa-Py catalyzed cascade oxidation–Knoevenagel condensation reactions from alcohols to α,β-unsaturated dinitriles[a]
 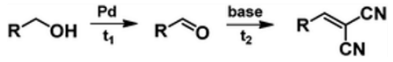
<table><tr><th>Entry</th><th>R</th><th>Time (h)
[t_1 + t_2]</th><th>Conv. (%)
A</th><th>Yield (%)
B</th><th>C</th></tr><tr><td>1</td><td>4-CH_3O–C_6H_5</td><td>4 + 1.5</td><td>99</td><td>Trace</td><td>99</td></tr><tr><td>2</td><td>4-CH_3–C_6H_5</td><td>4 + 1.5</td><td>98</td><td>Trace</td><td>97</td></tr><tr><td>3</td><td>4-NO_2–C_6H_5</td><td>7 + 2</td><td>92</td><td>Trace</td><td>91</td></tr><tr><td>4</td><td>4-Cl–C_6H_5</td><td>6 + 2</td><td>96</td><td>Trace</td><td>94</td></tr><tr><td>5</td><td>3-Cl–C_6H_5</td><td>6 + 2</td><td>93</td><td>Trace</td><td>93</td></tr><tr><td>6</td><td>n-C_6H_{13}</td><td>12 + 5</td><td>91</td><td>Trace</td><td>91</td></tr><tr><td>7</td><td>n-C_8H_{17}</td><td>12 + 5</td><td>94</td><td>Trace</td><td>93</td></tr></table>a Reaction conditions: a mixture of alcohol (1 mmol), toluene (10 mL), and Pd/COF-TpPa-Py was stirred at 80 °C under O_2 (1 atm) for t_1 h and then malononitrile (1.05 mmol) was introduced, and the reaction continued for t_2 h.</td><td>S31</td></tr>
<tr><td>2</td><td> 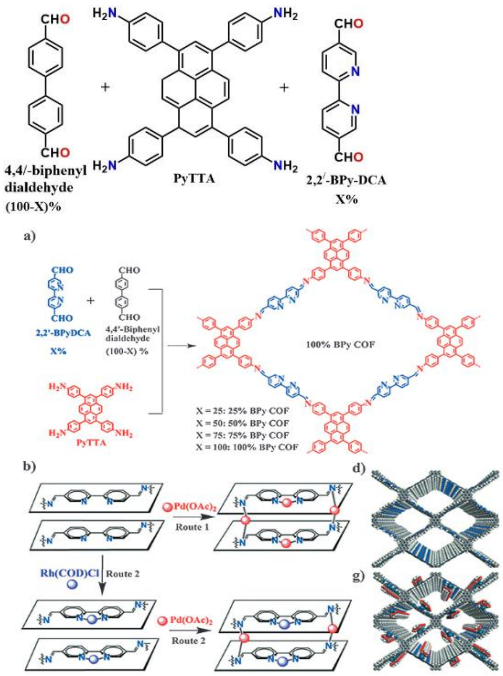
Mixed building blocks aare used to fabricate different COFs. The BET surface areas range from 500 to 1300 m^2/g. Rh is in (I) and Pd is in (II) oxidation states. ICP-OES: Rh loadings were 4.9, 7.8, 7.5 and 7.9 wt %, for systematically varying concentration (25, 50, 75 and 100) of 2,2’bpy unit in the COF. ICP-OES: Pd loading was 8.5, 9.1, 8.0 and 10.7 wt % with X values of 25, 50, 75 and 100, respectively. Active species: Rh(I) and Pd(II). Reprinted with the permission from the Wiley Online Library (reference S32).</td><td> 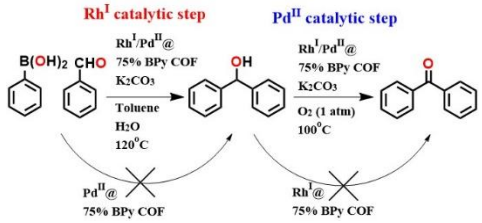
Rh/Pd containing COF catalyses both the steps with >90% yields.
<table><tr><th>Catalyst</th><th>Yield of addition reaction [%][a]</th><th>Yield of oxidation reaction [%][b]</th><th>Yield of cascade reaction [%][c]</th></tr><tr><td>Rh^I/Pd^{II}@75 % BPy COF 4th cycle</td><td>–</td><td>–</td><td>87</td></tr><tr><td>Rh^I/Pd^{II}@75 % BPy COF 5th cycle</td><td>–</td><td>–</td><td>85</td></tr><tr><td>Rh^I@75 % BPy COF</td><td>88</td><td>0</td><td>0</td></tr><tr><td>Pd^{II}@75 % BPy COF</td><td>0</td><td>99</td><td>0</td></tr><tr><td>Rh(COD)Cl+Pd(OAc)$_2$[e]</td><td>–</td><td>–</td><td>3</td></tr><tr><td>Rh(COD)Cl+Pd(OAc)$_2$ +bipyridine ligand[f]</td><td>–</td><td>–</td><td>99</td></tr></table>[a] Phenylboronic acid (2.0 mmol), benzaldehyde (1.0 mmol), potassium carbonate (3.0 mmol), catalyst (containing 0.01 mmol metal), toluene/H_2O (15 mL/5 mL), 120 °C, 24 h, N_2 protection. [b] Diphenylmethanol (1.0 mmol), potassium carbonate (3.0 mmol), catalyst (containing 0.01 mmol of metal), toluene/H_2O (15 mL/5 mL), ambient air, 100 °C, 12 h. [c] After the addition reaction, the temperature was decreased to 100 °C and O_2 was purged. [d] The catalyst was filtered and reused. [e] Rh(COD)Cl (0.01 mmol) and $Pd(OAc)_2$ (0.01 mmol) as homogeneous catalyst. [f] Rh(COD)Cl (0.01 mmol), $Pd(OAc)_2$ (0.01 mmol), and bipyridine ligand (0.02 mmol) as homogeneous catalyst.</td><td>S32</td></tr>
</table>

3	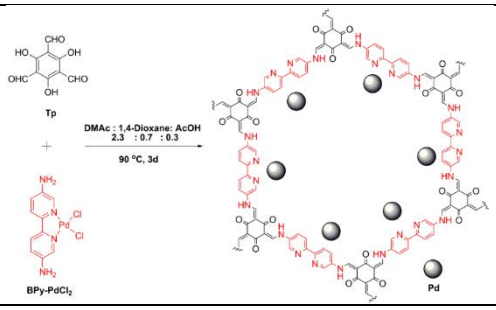	 R1: -NO_2, F, -CN, -OMe etc. R2: -NMe_2, -CMe_3, Me, -CN, F, -OMe etc. Yield: ~70% TON: ~1101	S33
Code: TpBpy. Bpy-$PdCl_2$ building block generates Pd nano particles in-situ during the COF formation. Surface area of TpBpy: **1462 m^2/g**. Pd@TpBpy: **653 m^2/g**. Average particle size: **12 ± 4 nm**. ICP-OES: Pd loading = **15.2 wt%**. Active species: **Pd(II).** Reprinted with the permission from the American Chemical Society (reference S33).			
Nitro reduction using noble metal nanoparticles @COF			
4	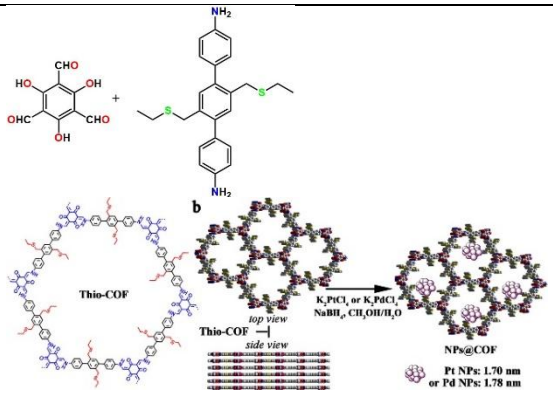	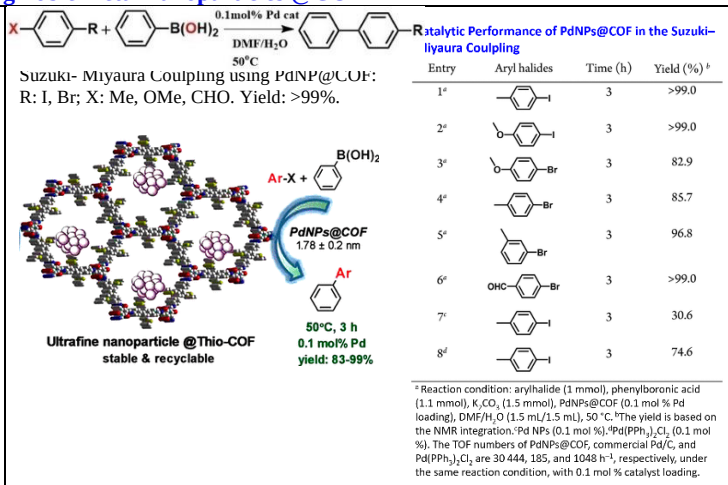 Suzuki- Miyaura Coulpling using PdNP@COF: R: I, Br; X: Me, OMe, CHO. Yield: >99%. Catalytic Performance of PdNPs@COF in the Suzuki–Miyaura Coulpling Entry / Aryl halides / Time (h) / Yield (%) [b] 1[a] 3 >99.0 2[a] 3 >99.0 3[a] 3 82.9 4[a] 3 85.7 5[a] 3 96.8 6[a] 3 >99.0 7[c] 3 30.6 8[d] 3 74.6 [a] Reaction condition: arylhalide (1 mmol), phenylboronic acid (1.1 mmol), K_2CO_3 (1.5 mmol), PdNPs@COF (0.1 mol % Pd loading), DMF/H_2O (1.5 mL/1.5 mL), 50 °C. [b]The yield is based on the NMR integration. [c]Pd NPs (0.1 mol %). [d]$Pd(PPh_3)_2Cl_2$ (0.1 mol %). The TOF numbers of PdNPs@COF, commercial Pd/C, and $Pd(PPh_3)_2Cl_2$ are 30 444, 185, and 1048 h^{-1}, respectively, under the same reaction condition, with 0.1 mol % catalyst loading. Nitro phenol reduction using $NaBH_4$ and PtNP@COF. 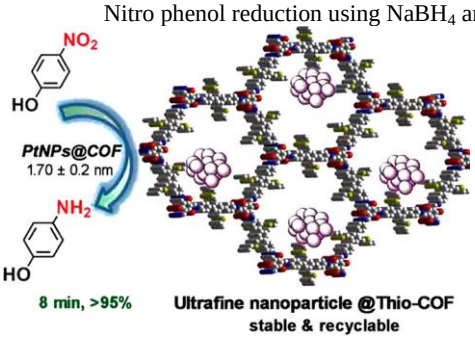	S34
The COF (Thio-COF) has relatively small surface area (**50 m^2/g**). The theoretical pore size is **2.4 nm**. The pore is decorated with thiol groups which are helping to grow ultra-small Pt and Pd nps (**< 2 nm**). From ICP: Pt loading= **34.36 wt %**; Pd loading= **26.30 wt %**; Active species: **Pd(0).** Reprinted with the permission from the American Chemical Society (reference S34).			
5	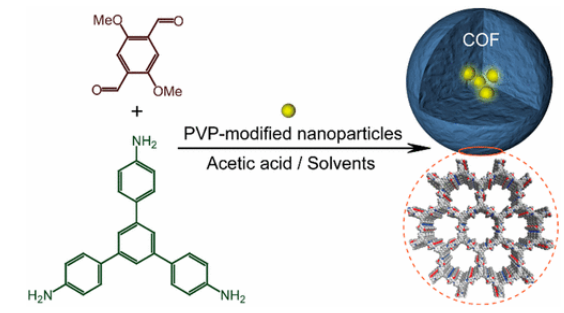	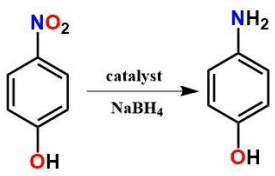 Nitro phenol reduction The acyivity is dependent on the nano rod size. The size increases, rate of reduction also increases. Au nP size: 15 nm and 50 nm particles; 25 x 100 nm Au rod. Rate of reduction 0.46 min^{-1} and TOF 2.7 h^{-1}.	S35

PVP modified Au nano-rods with different sizes are grown in the COF during synthesis. BET surface areas are greater than **2000 m^2/g** for the COF and Au nano-rod incorporated COFs. ICP: **0.2 wt%** loading for 15 nm Au; **0.26 wt%** for Au rods; **0.38 wt%** for 50 nm Au particles. Active species: **Au(0).** Reprinted with the permission from the American Chemical Society (reference S35).			
6	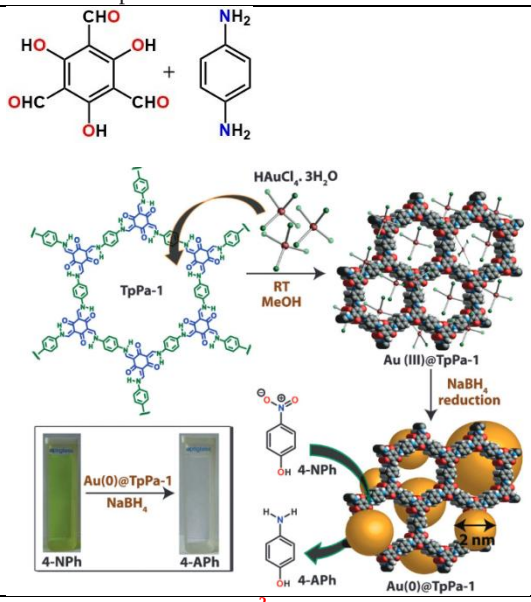	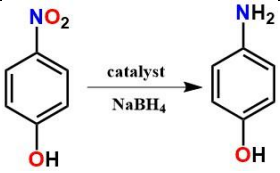 Nitro phenol reduction Conversion is >99%. 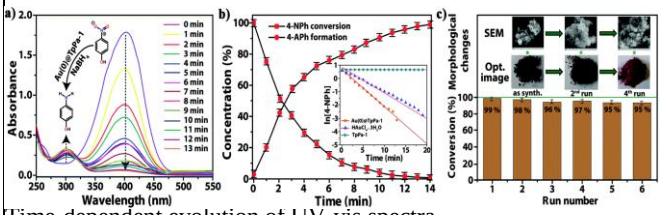 Time-dependent evolution of UV-vis spectra Kinetics of the reduction reaction of 4-NPh to 4-APh Cycling stability. Note the color change.	S36
BET surface area: TpPa-1: **484 m^2/g** and Au@TpPa-1 is **339 m^2/g**. The particle size distribution is **5 ± 3 nm**. Active species: **Au(0).** Reprinted with the permission from the Royal Society of Chemistry (reference S36).			
7	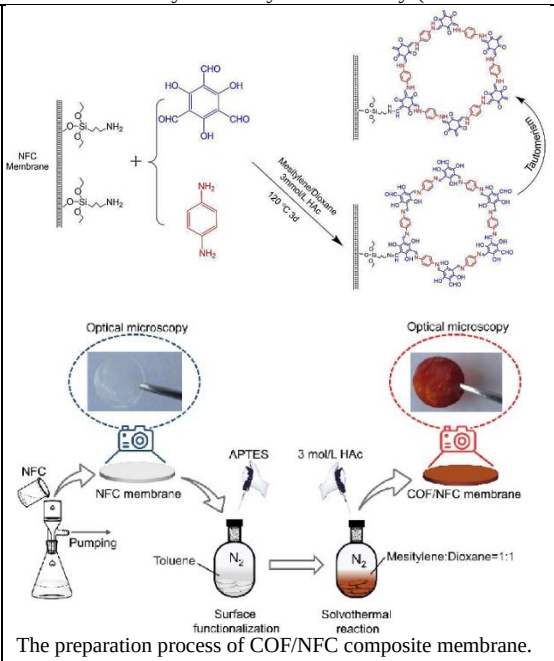 The preparation process of COF/NFC composite membrane.	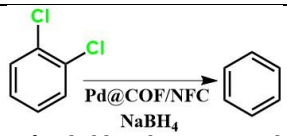 Catalytic dechlorination of o-dichloro benzene. High catalytic activity is observed with a rate constant of 0.0235 min^{-1}. 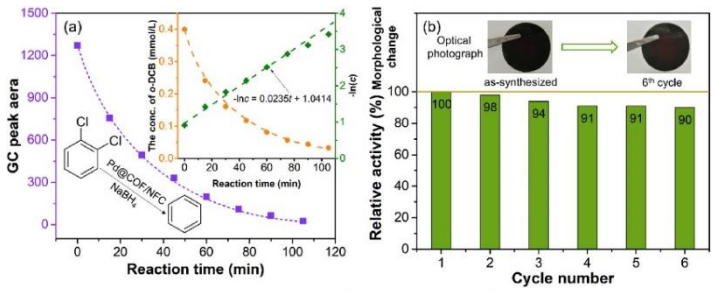 (a) Violet: Time-dependent evolution of GC peak area of o-DCB showing the catalytic reduction of *o*-DCB by Pd@COF/NFC, orange: plot of *o*-DCB concentration over time, olive: kinetics of the reduction reaction of *o*-DCB to benzene. (b) Top: the morphological change of the composite membrane after cyclic catalysis, bottom: the relative activity of Pd@COF/NFC catalyst during 6 cycles of reaction. Note the slight change in colour of the membrane after the 6th cycle.	S37
Nanofibrillated Cellulose is blended with COF. The composite has BET surface area **357 m^2/g**, pore size **2-20 nm** and the thickness of the membrane is **250 nm**. EDAX: **12.62%** of Pd loaded in the COF-NFC composite. Active species: **Pd(0).** Reprinted with the permission from the Elsevier (reference S37).			

8	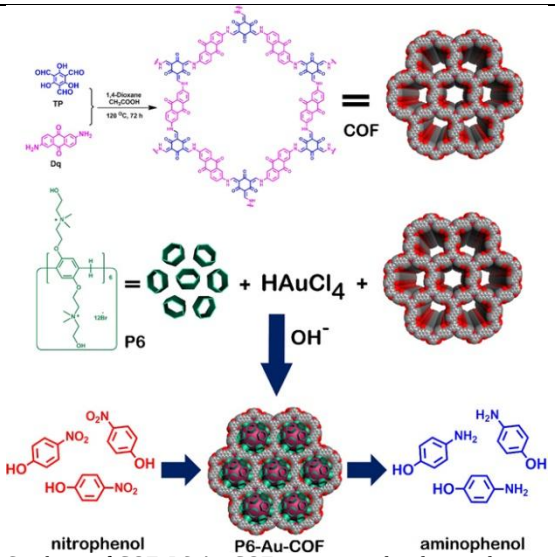 Synthesis of COF, P6-Au-COF nanomaterial and its application in the catalyzing reduction of nitrophenol isomers.	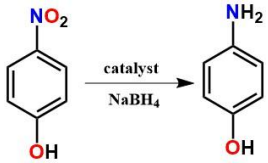 Reduction of nitroaromatic by $NaBH_4$. 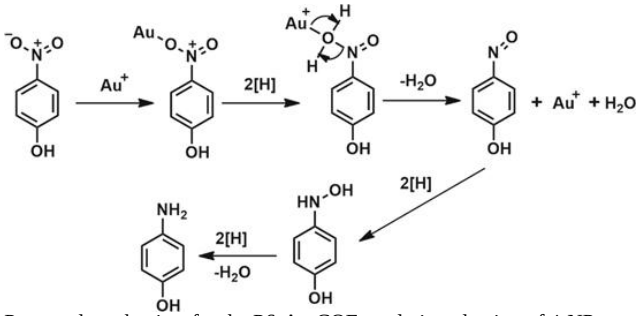 Proposed mechanism for the P6-Au-COF catalytic reduction of 4-NP.	S38
BET SA for COF is **685 m^2/g** and pillar[6]arene containing COF has **328 m^2/g** surface area. Average size of the Au is **2-3 nm**. Active species: **Au(0).** Reprinted with the permission from the IOP Science (reference S38).			
9	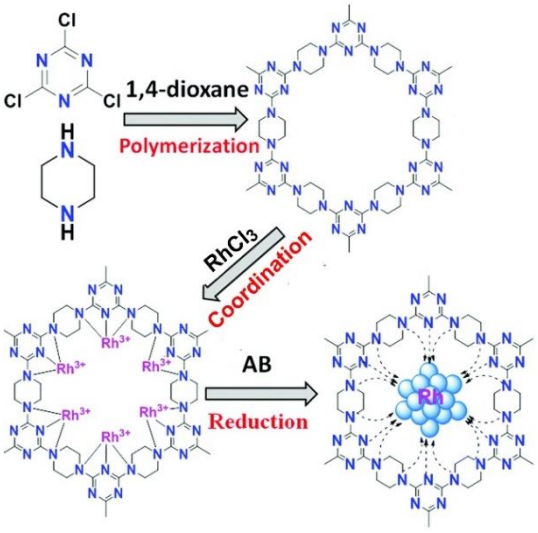	$NH_3BH_3 + 2H_2O \rightarrow NH_4BO_2 + 3H_2$ (1) $NH_3BH_3 + 4CH_3OH \rightarrow NH_4B(CH_3O)_4 + 3H_2$ (2) TOF for the reaction is 505 min^{-1} at 298K. Electron-rich ultrafine Rh nano particles. Activation energy is 31.8 kJ/mol. 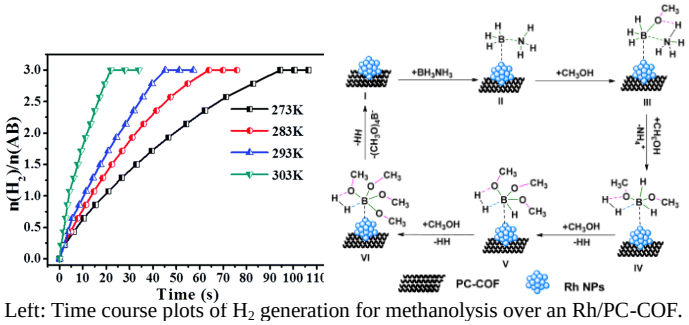 Left: Time course plots of H_2 generation for methanolysis over an Rh/PC-COF. Right: A plausible mechanism of AB methanolysis catalyzed by the Rh/PC-COF.	S39
BET SA of the PC-COF is **389 m^2/g** and Rh/PC-COF is **268 m^2/g**. Pore size **3.5-3.7 nm** for both the materials. Average particle size of Rh nano particle is **2±0.4 nm**. ICP: **0.96 wt%** Rh loading. Active species: **Rh(0).** Reprinted with the permission from the Royal Society Chemistry (reference S39).			

10	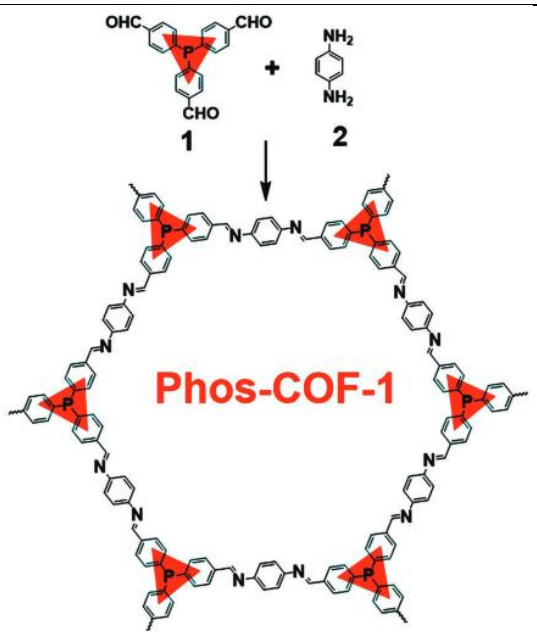	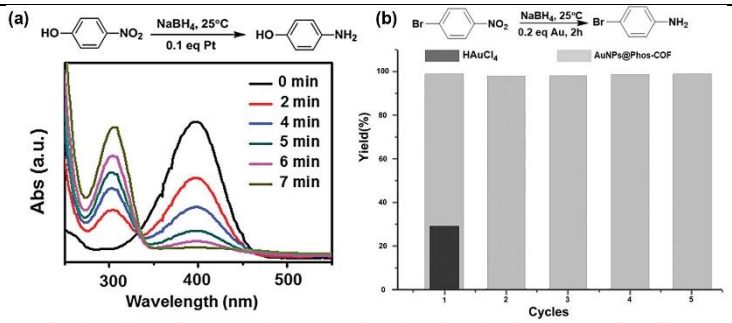 (a) The time-dependent UV–vis spectra of 4-nitrophenol reduction catalyzed by 0.1 eq. PtNPs@Phos-COF-1. (b) Catalytic performance of Au catalyst (0.2 eq) in the reduction reaction. 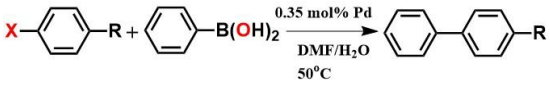 Suzuki–Miyaura coupling reaction. R: Me, OMe, NO_2, CHO and X: I, Br. Yield >99%. TOF is 155-1648 h^{-1} for the Suzuki–Miyaura coupling reaction. 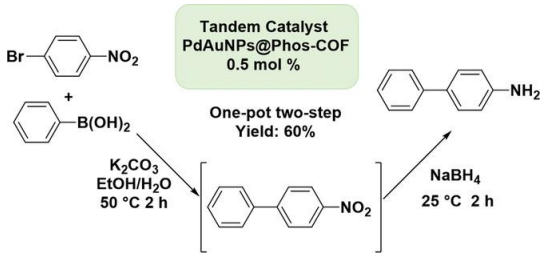 The one-pot two-step tandem cross-coupling and hydride reduction under the catalysis of PdAuNPs@Phos-COF-1.	S40
BET surface area: **818 m^2/g** (pore size: **1.56 nm**). A broad scope of growing small-sized nano particles is studied. Average particle sizes: PdNPs@Phos-COF-1 = **1.62±0.37 nm**, PtNPs@Phos-COF-1 = **2.06±0.54 nm**, AuNPs@Phos-COF-1 = **1.78±0.32 nm** and PdAuNPs@Phos-COF-1 = **1.03±0.07 nm**. PPh_3 core helps to generate small-sized nano clusters in the COF. ICP: The Pd, Pt, and Au contents were **2.8%, 3.2%,** and **12.5 wt%**, respectively. Active species: **Pd(0), Pt(0)** and **Au(0).** Reprinted with the permission from the Wiley Online Library (reference S40).			
11	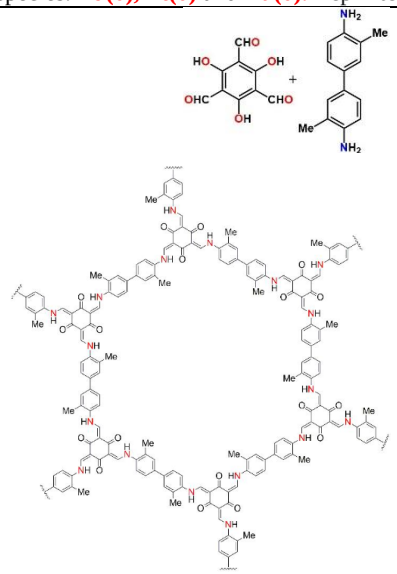	$HCOOH \longrightarrow CO_2 + H_2$ Selective formic acid dehydrogenation. 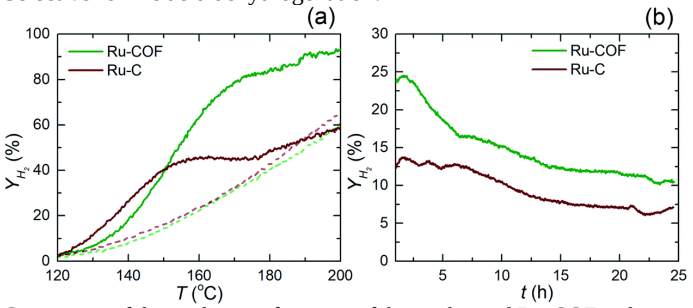 Comparison of the catalytic performance of the synthesized **Ru-COF** and commercial **Ru–C** control catalyst in the dehydrogenation of FA. Light-off curves for (a) H_2 yield (Y_{H2}) as a function of reaction temperature; (b) stability test performed at 120 °C for 25 h, monitoring Y_{H2} as a function of time.	S41
BET SA of TpBD-Me_2 COF is **520 m^2/g** (pore size **1 nm**) and Ru-COF **630 m^2/g** (pore size **1.3 nm**). During recation, the RuO_2 nps are reduced to Ru nps. Average particle size of Ru is **~1.2nm**. ICP-OES: Ru loading is **2.4%**. Active species: **Ru(IV), Ru(0).** Reprinted with the permission from the Royal Society of Chemistry (reference S41).			

12	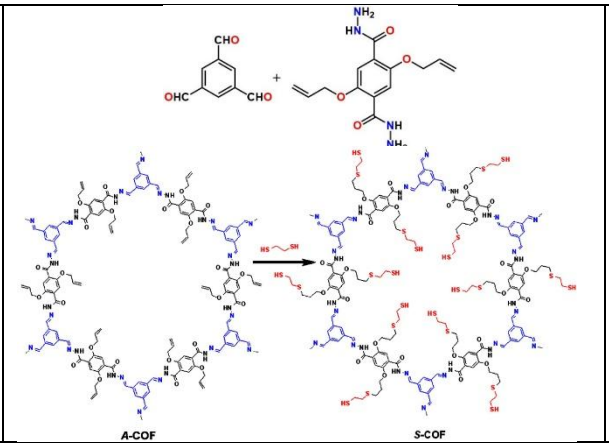	Nitrophenol reduction using Au@COF and $NaBH_4$ in < 10 mins. 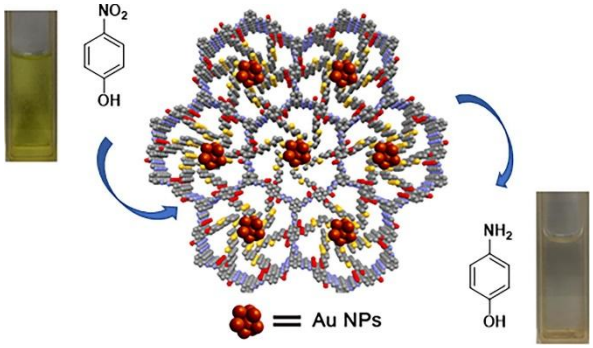	S42
Thiol decorated COF helps to grow small-sized Au nano particles. BET SA of A-COF and S-COF are **82** and **31 m^2/g**. The pore size of A-COF is **19 Å**. Au nanoparticle average particle size = **4.2 nm**. Atomic Absorption Sepctroscopy (AAS): **24 wt%** Au loaded in COF. Active species: **Au(0).** Reprinted with the permission from the Elsevier (reference S42).			
13	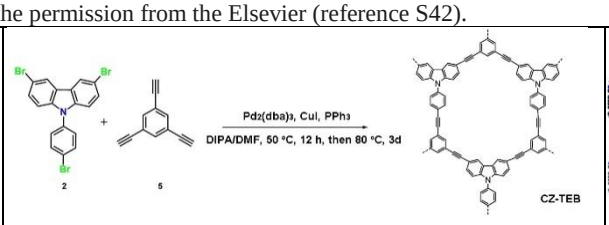	Ag@COF catalyzed Nitrophenol Reduction with $NaBH_4$ 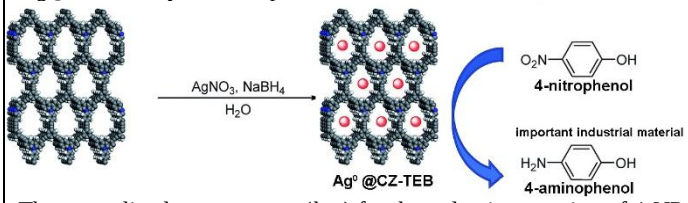 The normalized rate constant (k_{nor}) for the reduction reaction of 4-NP to 4-AP reaches up to 21.49 $mmol^{-1}$ s^{-1}.	S43
Covalent Carbazole framework with BET surface area of **1600 m^2/g**. The CZ-TEB has heirarchial porosity ranging from **1** to **10 nm**. Ag(0) nanoparticles have an average size of **2-4 nm**. ICP-AES: Ag loading = **5.1 wt%**. Active species: **Ag(0).** Reprinted with the permission from the Royal Society of Chemistry (reference S43).			
14	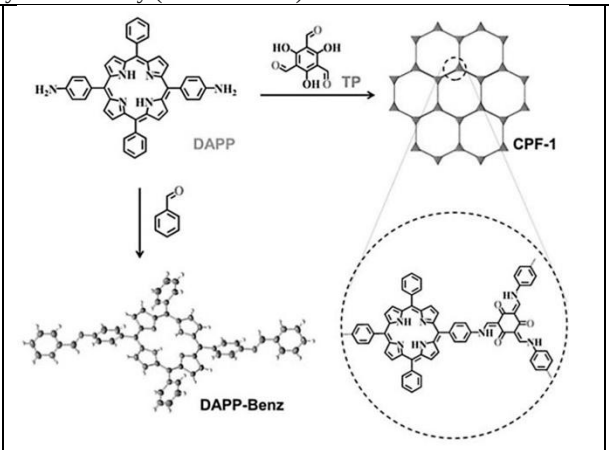	Au@COF catalyzed Nitophenol reduction in presence of $NaBH_4$. 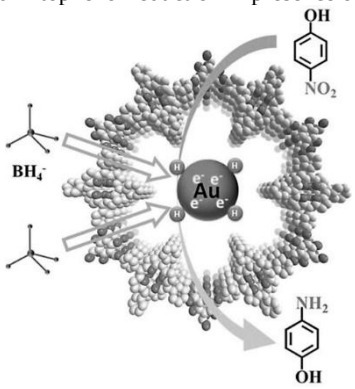 Mechanism of reduction of the nitrophenol on the Au surface by the $NaBH_4$.	S44
BET surface areas of CPF-1 (pore size **10-30 Å**) and Au@CPF-1 (pore size **8-25 Å**) are **192** and **150 m^2/g**. Average particle size of Au nano particles is **4-7 nm**. EDAX: **1.2 wt%** of Au loaded in COF. ICP-OES: **1.24 wt%** of Au in COF. Active species: **Au(0).** Reprinted with the permission from the Wiley Online Library (reference S44).			
Suzuki- Miyaura Coulpling			
15	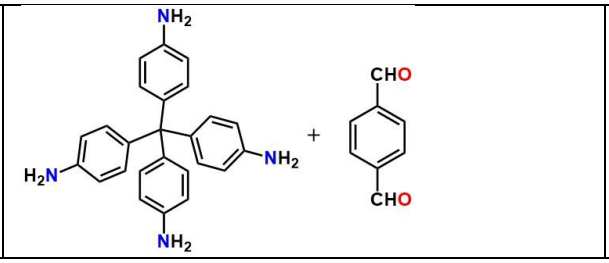	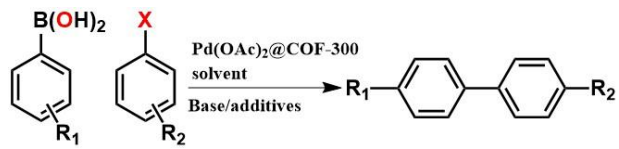 Suzuki- Miyaura Coulpling, R1, R2: aliphatic and aromatic groups, X: I, Br, Yield: ~50-100%, TON: 400-1000 and TOF: 50-3000 h^{-1}.	S45

	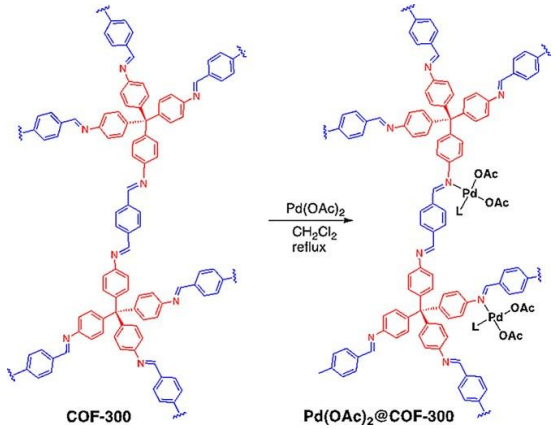	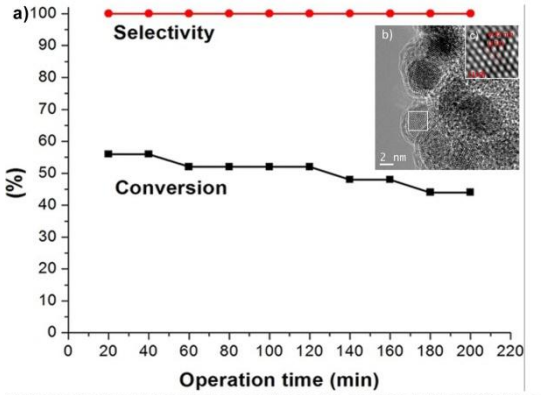 Continuous-flow Suzuki–Miyaura cross-coupling reaction employing Pd(OAc)2@COF300 as heterogeneous catalyst. Bromobenzene (squares) conversion to biphenyl (circles) as a function of time on stream. Inset shows the HRTEM image displaying the < 2 nm Pd(0) nPs.	
BET SA: **1373 m^2/g** (for COF-300), **270 m^2/g** (for $Pd(OAc)_2$@COF-300). From ICP-MS: Pd loading = **85 ppb**. Active species: **Pd(II) -> Pd(0).** Reprinted with the permission from the Wiley Online Library (reference S45).			
16	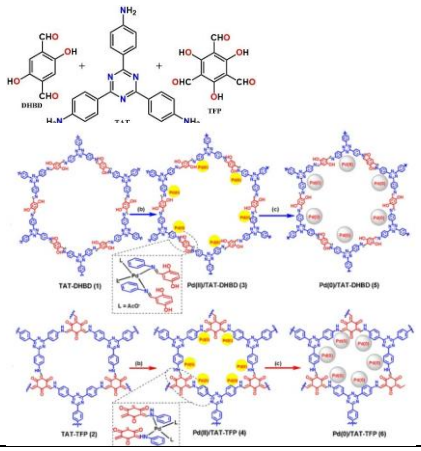	Suzuki-Miyaura coupling reaction  R: H, CH_3, OCH_3, CN. Pd loading from EDAX: 10.5 wt % in Pd^{II}/TAT-DHBD (**3**) 14.9 wt% in Pd^{II}/TAT-TFP (**4**), 11.4 wt% in Pd^0/TAT-DHBD (**5**) 10.6 wt % in Pd^0/TAT-TFP (**6**). Better yield and selectivity are obtained for -CN substituted starting materials. Yield = ~55-100%.	S46
Mixed-building units-based imine-COF. BET SA for TAT-DHBD and TAT-TFP are **750** and **646 m^2g^{-1}**. Major pore sizes are **29.1, 37.9 Å** (TAT-DHBD) and **11.7 Å** (TAT-TFP). Active species: **Pd(0).** Reprinted with the permission from the Wiley Online Library (reference S46).			
17	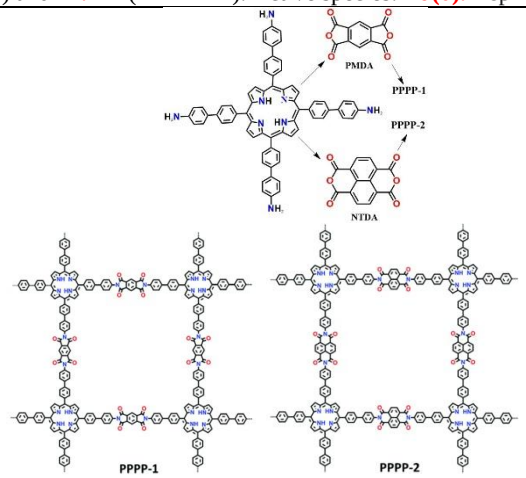	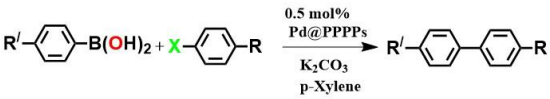 Suzuki-Miyaura coupling reaction. Yield: >90%. 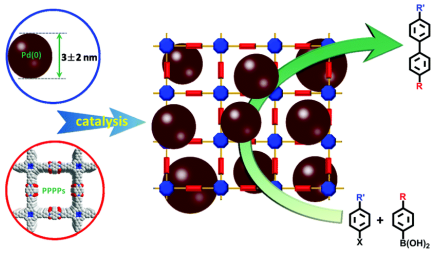	S47
BET SA: PPPP-1: **295 m^2/g** (pore size **1.3-2.9 nm**); Pd@PPPP-1: **198 m^2/g** (pore size **1.5-2.6 nm**); PPPP-2: **301 m^2/g** (pore size **1.6-3.3 nm**); Pd@PPPP-2: **210 m^2/g** (**1.7-2.9 nm**); Average particle size of Pd nps is **3 ± 2 nm**. ICP-OES: Pd in PPPP-1 = **3.58 wt%**; Pd in PPPP-2 = **3.63 wt%**. Active species: **Pd(0).** Reprinted with the permission from the Royal Society of Chemistry (reference S47).			
18		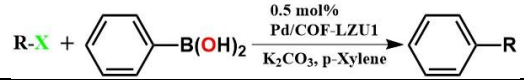	S48

	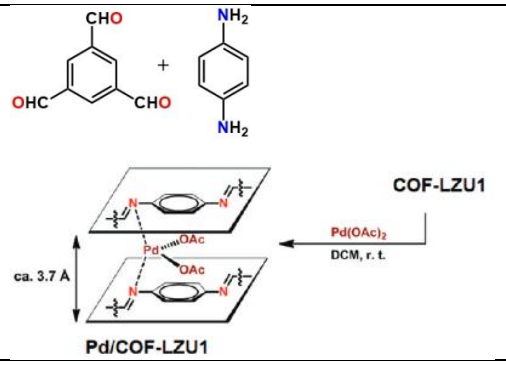	Suzuki-Miyaura Coupling Reaction. R: Aromatic groups with EDG and EWG substitution. Yield > 95%. 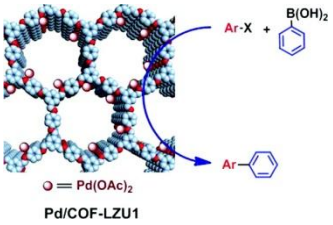	
Surface areas of COF-LZU1 and Pd/COF-LZU1 are **410** and **146 m^2/g**, respectively. ICP: Pd loading in Pd/COF-LZU1 **~7.1 ± 0.5 wt %**. Active species: **Pd(II).** Reprinted with the permission from the American Chemical Society (reference S48).			
19	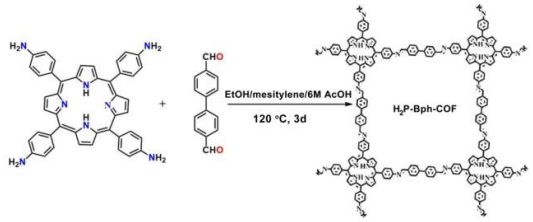	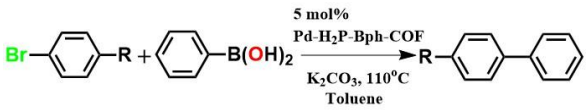 Suzuki coupling reaction. R: CHO, NO_2, $COOCH_3$, CN , CH_2OH, OH, NH_2, $C(CH_3)_3$ etc. Yield: >90%	S49
BET SA: H_2P-Bph-COF and Pd/H_2P-Bph-COFwere **550** and **147 m^2/g**. Both have **2.96** nm pore size. ICP-AES: Pd loading **2.87%**. Active species: **Pd(II).** Reprinted with the permission from the Elsevier (reference S49).			
20	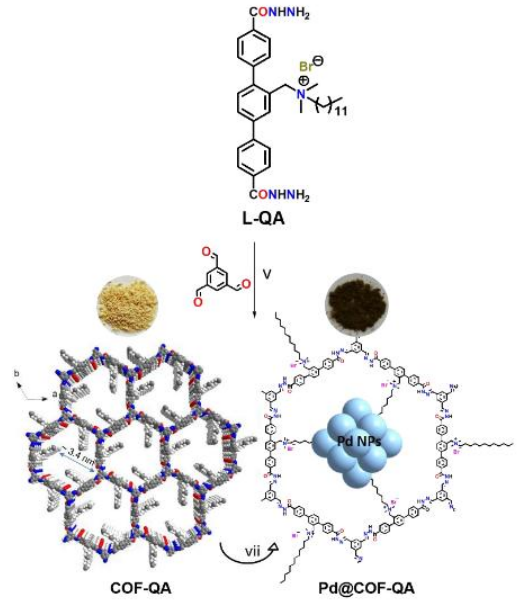 The COF is decorated with quarternary ammonium salt.	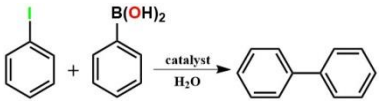 Suzuki-Miyaura coupling reaction in water. The quarternary ammonium salt decorated COF synergistically grows small-sized Pd nano particles and acta as a phase transfer catalyst which helps the rection to proceed in aqueous condition. 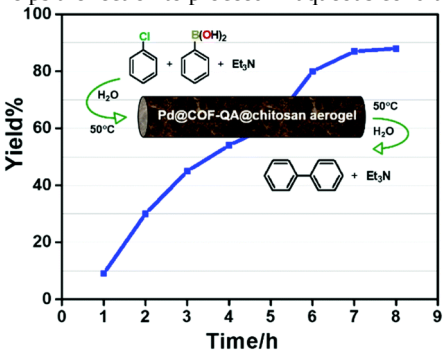 Dispersing the Pd@COF into chitosan generates aerogen which acts as a composite catalyst.	S50
The average size of the Pd nano particles are **2.4 nm**.The COF-QA and Pd@COF-QA have surface areas of **59** and **26 m^2/g**. ICP: Pd loading in the Pd@COF-QA = **9.2 wt%**. Active species: **Pd(0).** Reprinted with the permission from the Royal Society of Chemistry (reference S50).			

21	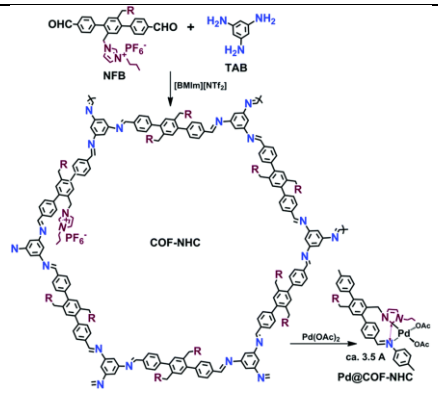	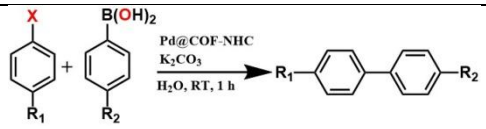 Suzuki-Miyaura Cross Coupling of Aryl Halide with Different Boronic Acids. R1: H, CH_3, OCH_3, NO_2 etc. R2: H, Cl, CH_3, OCH_3. X: Br, I. Yield: >95%. 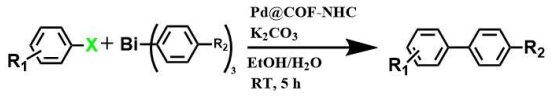 Crosscoupling reaction of triarylbismuths and aryl halides. Yield: > 80%. R_1: 3-NH_2, 4-NH_2, 4-CH_3, 4-OCH_3, Cl, 4-NO_2, 4-CN etc. R_2: H, 4-CH_3, 4-OCH_3	S51
The COF is decorated with N-heterocyclic carbene. The nitrogen centres are coordinating to the Pd^{2+} ions. BET SA of COF-NHC is **45 m^2/g (**Mean pore size: **2.70 nm**. ICP: Pd loading in the COF = **20.1 wt%**. Active species: **Pd(II).** Reprinted with the permission from the Royal Society of Chemistry (reference S51).			
22	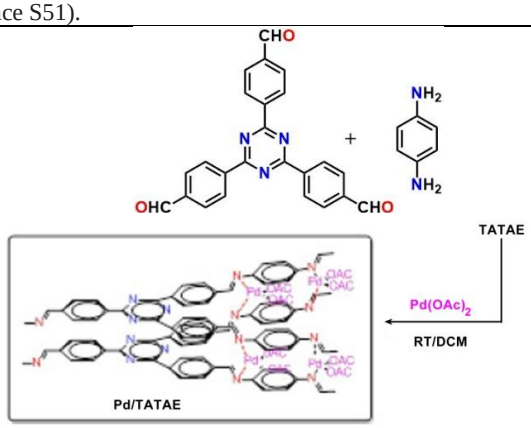	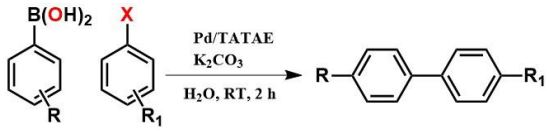 Suzuki-Miyaura coupling under aq. Condition. R: H, 4-CHO, 4-OMe, 4-Me R1: H, NH_2, CN, 2-NO_2, 4-CHO, 4-Me, 2-NH_2 etc. X: I, Br. Yield: >90% TON: >1000	S52
BET surface areas of ATAE and Pd/TATAE are **160** and **104 m^2/g**. Pore size is **7.6 Å**. Active species: **Pd(II).** Reprinted with the permission from the Wiley Online Library (reference S52).			
Sonogashira coupling, and Heck coupling reactions			
23	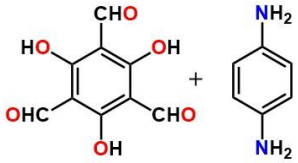	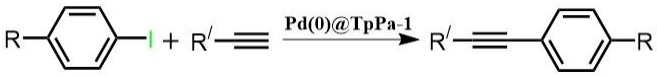 Sonogashira coupling between aryl iodides and aromatic/aliphatic alkynes. R: H, Me, OMe, CF_3, NO_2, CO_2H R`: Ph, CH_2OH, ^{t}BuSi. Yield: ~50%; TON: ~300, TOF: ~50 h^{-1}  Heck coupling reaction between aryl iodides and aromatic/aliphatic olefins. R: H, Me, OMe, CF_3, NO_2, I R`: Ph, CH_2OH, ^{t}BuOCO. Yield: ~90%; TON: ~300, TOF: ~50 h^{-1} 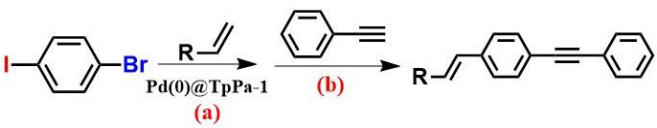 One-pot sequential Heck/Sonogashira coupling reactions of aryl dihalides. R: Ph, ^{t}BuOCO.	S53

	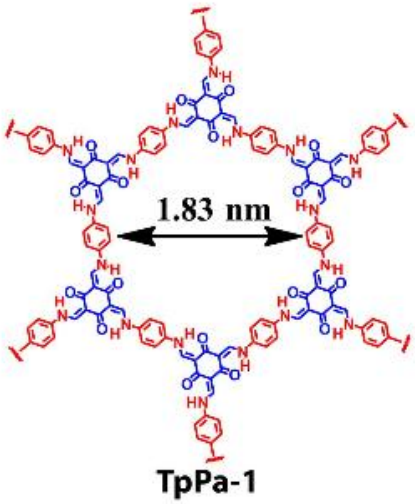	Yield: 62% and 85%; TON: 66 and 73, TOF: 11 and 12 h^{-1}	
BET surface area for the neat COF is **484 m^2/g**. Pd(OAc) was loaded into the COF followed by $NaBH_4$ reduction generates Pd(0) nano particles (**4±2 nm**). From EDX analyses: **Pd(0)@TpPa-1** has a Pd(0) loading of **6.4 wt%** and **Pd(II)@TpPa-1** has a Pd(II) loading of **10.2 wt%**. Active species: **Pd(0).** Reprinted with the permission from the Royal Society of Chemistry (reference S53).			
24	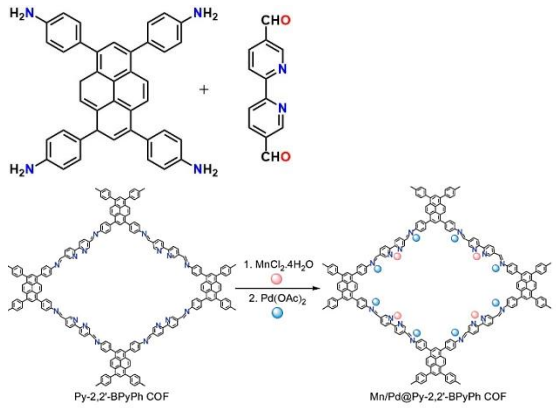	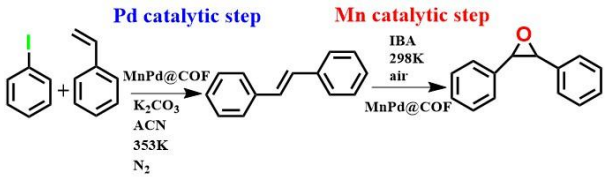 Both the steps yield >90% of the products. 	S54
BET surface area of the COF is **2038 m^2/g** (pore size **2.6 nm**). Mn@COF is **1711 m^2/g** (pore size **2.6 nm**). MnPd@COF is **1562 m^2/g** (pore size **2 nm**). ICP-OES: Mn content of Mn@Py-2,20-BPyPh COF was **0.8 wt%**. In comparison, the Mn and Pd content of Mn/Pd@Py-2,20-BPyPh COF were **0.8 wt%** and **9.3 wt%**, respectively. Thus, the pre-loaded Mn was neither lost nor replaced by subsequently loaded Pd. Active species: **Mn(II), Pd(II).** Reprinted with the permission from the Royal Society of Chemistry (reference S54).			
25	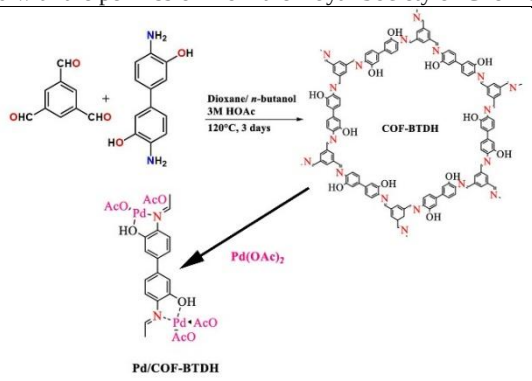	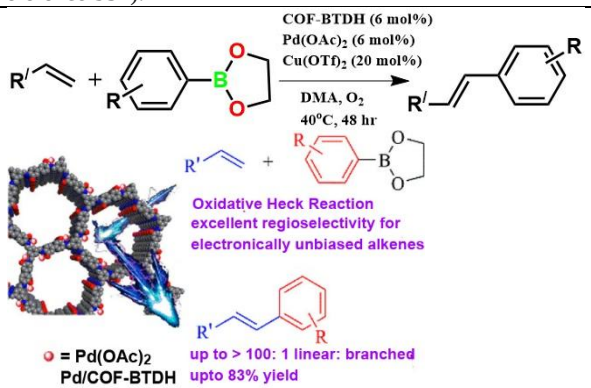 Copper salt effectively facilitate transmetalation	S55
Surface area for COF-BTDH and Pd/COF-BTDH are **91** and **65 m^2/g**. The average pore size ranges in **2-3 nm** for bot the COF and the composite. ICP:			

Pd loading = **5.13 wt%**. Active species: **Pd(II).** Reprinted with the permission from the American Chemical Society (reference S55).

26

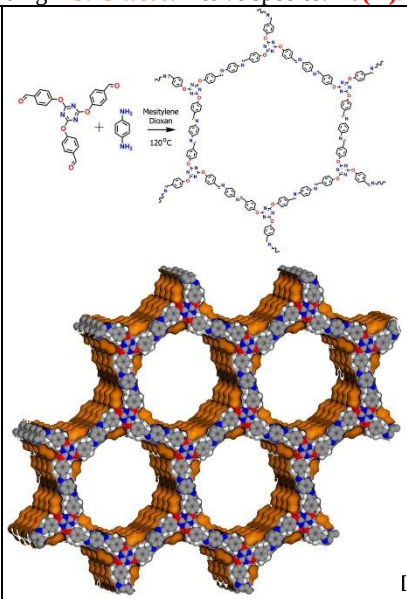

IISERP-COF1

The presence of hydrophobic ether bonds and hydrophilic triazine units present an amphiphilic environment. This is evident from improved adsorption for methanol over toluene and water. Also, from the contact angles. The amphiphilic enviroment typically supports stabilizing Pd(0) as well as Pd^{2+} in mixed-solvent homogeneous medium.

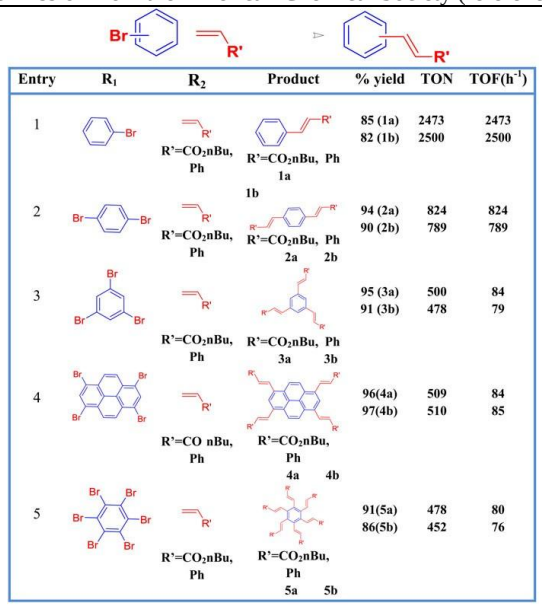

Entry	R_1	R_2	Product	% yield	TON	TOF(h^{-1})
1		R'=CO_2nBu, Ph	R'=CO_2nBu, Ph 1a / 1b	85 (1a) 82 (1b)	2473 2500	2473 2500
2		R'=CO_2nBu, Ph	R'=CO_2nBu, Ph 2a 2b	94 (2a) 90 (2b)	824 789	824 789
3		R'=CO_2nBu, Ph	R'=CO_2nBu, Ph 3a 3b	95 (3a) 91 (3b)	500 478	84 79
4		R'=CO nBu, Ph	R'=CO_2nBu, Ph 4a 4b	96(4a) 97(4b)	509 510	84 85
5		R'=CO_2nBu, Ph	R'=CO_2nBu, Ph 5a 5b	91(5a) 86(5b)	478 452	80 76

Multi-fold Heck-coupling results in industrially valuable monomers for several styrene-based polymers. The Pd@COF catalyzes CO oxidation even at 180°C with a light off temperature at 140 °C and drastic increase in activity to full conversion at 160 °C. This highlights their stability to harsh conditions. The Pd@COF has been developed into membranes by compositing with PMMA.

S56

BET SA: IISERP-COF1 = **408.5 m^2/g**; Pd@IISERP-COF1 = **404 m^2/g**. BJH pore size: IISERP-COF1 = **23 Å**; Pd@IISERP-COF1 = **19 Å**. Pd nP size: **5 to 20 nm**. EDAX: Pd loading = **18-20 wt%**. Active species: **Pd(0).** Reprinted with the permission from the Nature Publishing Group (reference S56).

CO_2 utilization

27

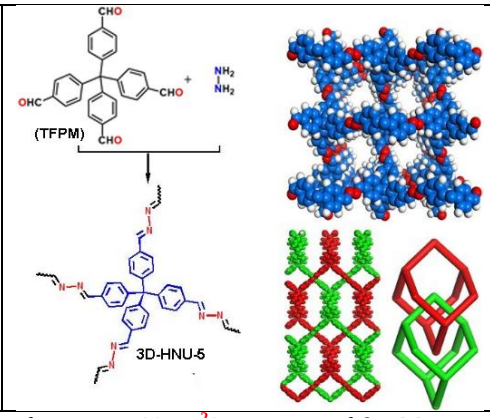

Chemical fixation of CO_2 to propargyl alcohols.

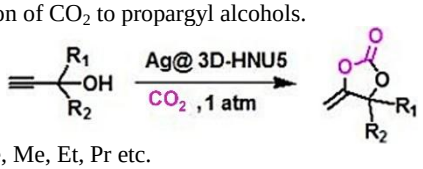

R1, R2: Me, Me, Me, Et, Pr etc.

Reaction conditions: propargylic alcohols (1.0 mmol), catalyst (0.1 mol%, based on loading of Ag), DBU (1.0 mmol), CH_3CN (3 mL), CO_2 (99.999%, balloon), RT, 12 h. The yields were determined by ^1H NMR spectroscopy.
Yield >99%
TON: 990

S57

BET surface area is **864 m^2/g**. Pore size of the COF is **1.01 nm**. The COF shows selective CO_2 capture (123.1 mg/g@273K, 1bar). Upon Ag loading the BET SA is **300 m^2/g** and CO_2 capacity drops to **83 mg/g**. Average particle size is **~1.7 nm**. EDX and ICP: Ag loading in COF = **2.32 wt%**. Active species: **Ag(0).** Reprinted with the permission from the Royal Society of Chemistry (reference S57).

28

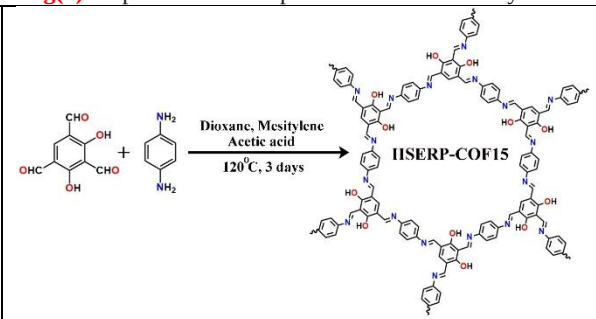

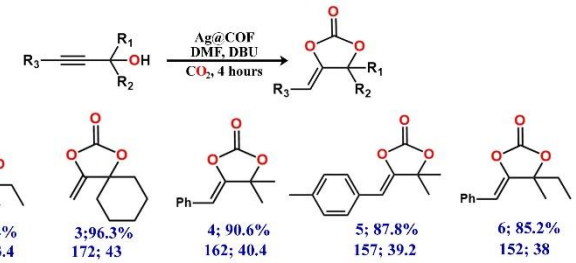

DBU is used as the base. 10 mol% catalyst is used for the reaction. 152-174 depending upon substrates.

S58

BET surface area of the COF is **1230 m^2/g**, DFT pore size is **12 Å**. **Ag(0)** is the catalytically active species. Ag loading is **6.3 wt%**. Average particle size is **3.3 nm**. Reprinted with the permission from the Wiley Online Library (reference S58).

Other important reactions (silicon based cross coupling, bezylic alcohol oxidation, bio catalysis, rearrangement etc.)

29	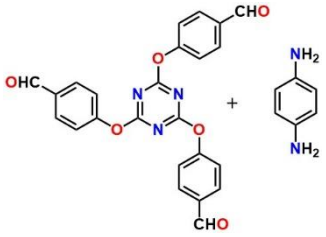	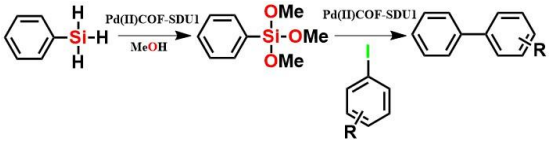 One-pot silicon-based cross-coupling reaction of silanes and aryl iodides. R: 4-CH_3, 2-CH_3, 4-OCH_3, 4-F, 4-OH, 4-NO_2. Yield: 70 to 90%.	S59

BET SA for COF-SDU1 and Pd(II)/COF-SDU1 are **1125** and **1052 m^2/g**. Pore sizes are **2.63** and **2.51**, respectively. Active species: **Pd(II).** Reprinted with the permission from the Royal Society of Chemistry (reference S59).

30	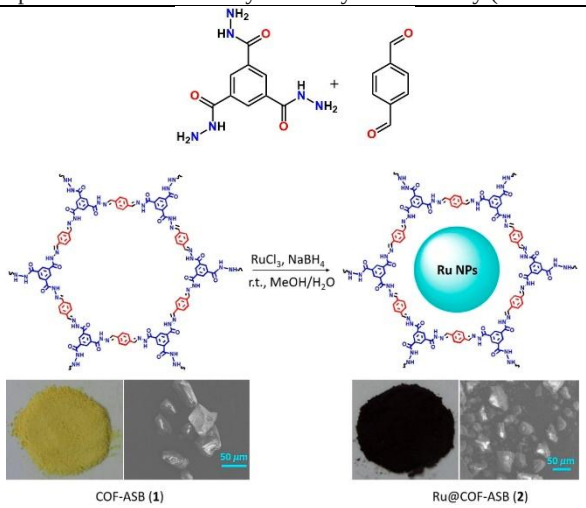	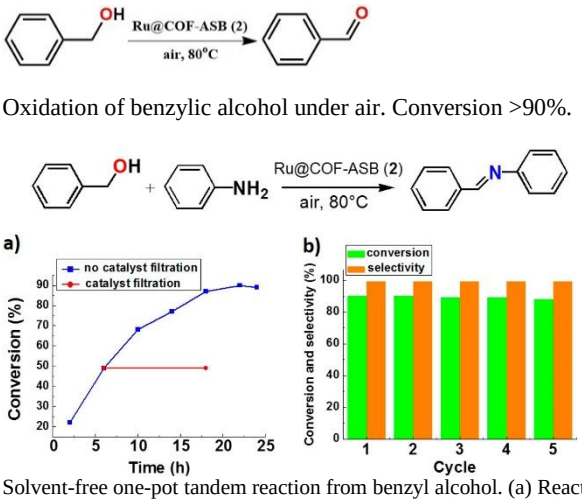 Solvent-free one-pot tandem reaction from benzyl alcohol. (a) Reaction time examination (black line) and leaching test (red line) for solvent free one-pot tandem synthesis of imine	S60

BET surface areas: COF-ASB is **233** and Ru@COF-ASB is **101 m^2/g**. Av. Particle size of Ru nps = **2-5 nm**. ICP: Ru loading = **4.1 wt%**. Active species: **Ru(0).** Reprinted with the permission from the American Chemical Society (reference S60).

31	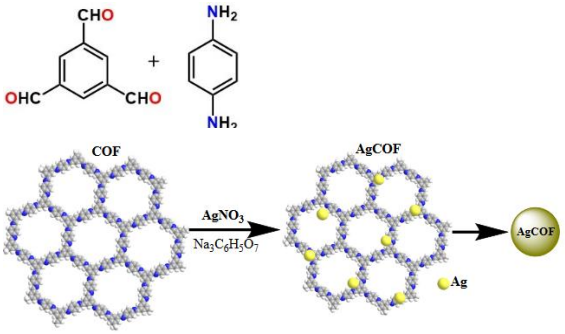 Sodium citrate generates the Ag nano particles.	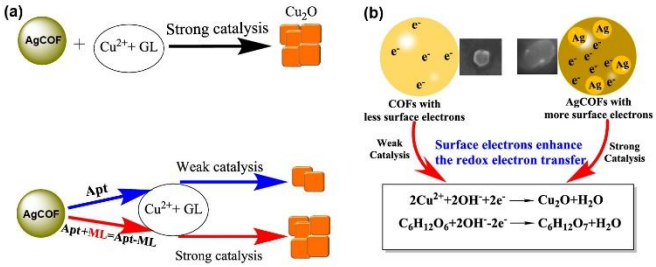 (a) Principle of the regulation of AgCOF catalysis of GL–Cu(II) by Apt to detect ML. (b) Principle of the catalytic enhancement of AgCOF.	S61

AgCOF is being prepared by the reduction of $AgNO_3$ using trisodium citrate solution. The Ag nano particles are grown on the COF surface. Reprinted with the permission from the American Chemical Society (reference S61).

32			S62

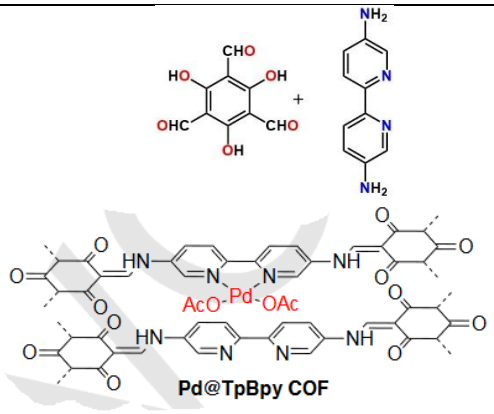

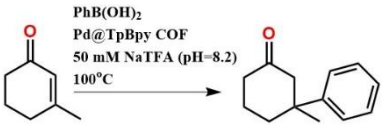

Conjugate Additions of Arylboronic Acids to β,β-Disubstituted Enones. Yield >99%.

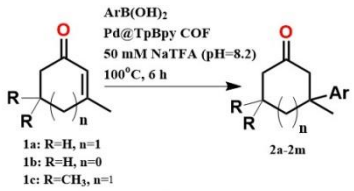

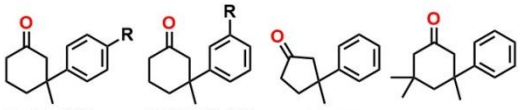

BET surface area of TpBpy COF is **578 m^2/g** and Pd@TpBpyCOF is **390 m^2/g**. Active species: **Pd(II).** Reprinted with the permission from the Wiley Online Library (reference S62).

33

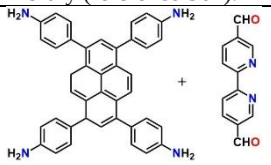

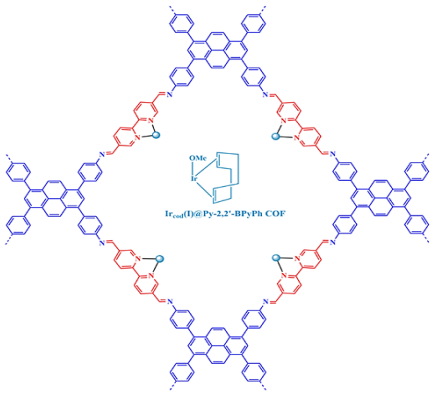

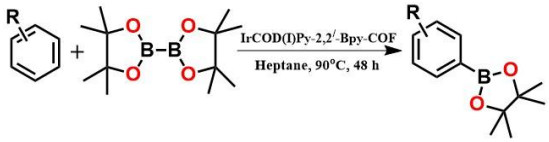

R: Cl, Br. CH_3, OCH_3, CF_3, pyrrole, thiophene.
Yield: 50-87%.

Entry	DCB:B_2Pin_2	Solvent	Temp (°C)	Catalyst	Yield (%)
1	1:0.5	THF	67	Ir_{cod}(I)@Py-2,2′-BPyPh COF	<5
2	1:0.5	DMF	40	Ir_{cod}(I)@Py-2,2′-BPyPh COF	<5
3	1:0.5	Heptane	90	Ir_{cod}(I)@Py-2,2′-BPyPh COF	66
4	1:1	Heptane	90	Ir_{cod}(I)@Py-2,2′-BPyPh COF	87
5	1:1	Heptane	90	[Ir(OMe)(cod)$_2$] + Py-2,2′-BPyPh COF	13
6	1:1	Heptane	90	[Ir(OMe)(cod)$_2$]	<5
7	1:1	Heptane	90	Py-2,2′-BPyPh COF	0

Effect of various catalysts and reaction conditions for preliminary C−−H borylation reaction. Reaction conditions: Ircod(I)@Py-2,2-BPyPh COF (0.6 mol. %, 0.008 mmol of iridium); arene:B s 2Pin2 (substrate to boron reagent molar ratio), 3 ml heptane. Yield was determined by 1H-NMR.

S63

BET SA for Py-2,2′-BPyPh COF and Ircod(I)s@Py-2,2′-BPyPh COF are **1785** and **859 m^2/g**. The pore sizes are **2.3** and **1.59 nm**. ICP: Ir loading = **3.1 wt%**. Active species: **Ir(I).** Reprinted with the permission from the American Institute of Physics (reference S63).

34	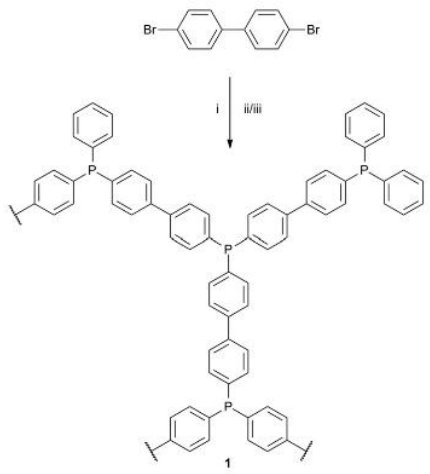	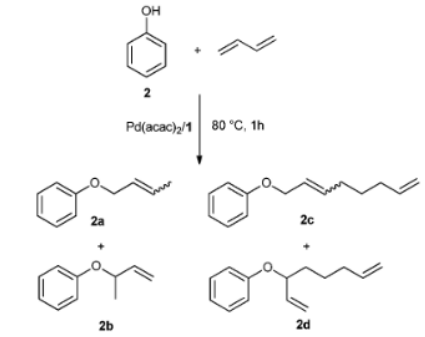 Telomerisation of 1,3-butadiene with Phenol. 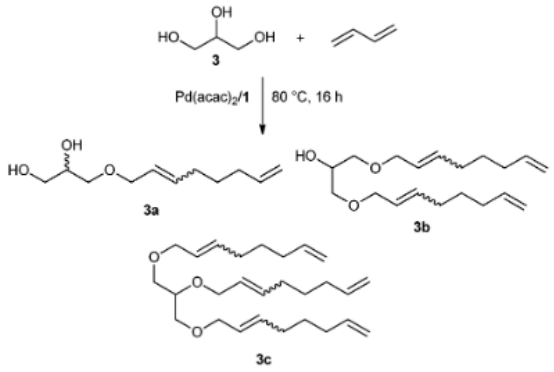 Telomerisation of 1,3-butadiene with glycerol.	S64
BET SA: **135 m^2/g**, pore volume of **0.04 cm^3/g**. BET SA after metal loading [$Pd(acac)_2$] is **58 m^2/g**. Reprinted with the permission from the Royal Society of Chemistry (reference S64).			

Note: Authors have taken the necessary rights and permissions from the concerned authorities/publishers prior to use their data or inputs.

References:

S1. Fang, Q.; Gu, S.; Zheng, J.; Zhuang, Z.; Qiu, S.; Yan, Y. 3D Microporous Base-Functionalized Covalent Organic Frameworks for Size-Selective Catalysis. *Angew. Chem. Int. Ed*. 2014, **126**, 2922 –2926.

S2. Li, H.; Pan, Q.; Ma, Y.; Guan, X.; Xue, M.; Fang, Q.; Yan, Y.; Valtchev, V.; Qiu, S. Three-Dimensional Covalent Organic Frameworks with Dual Linkages for Bifunctional Cascade Catalysis. *J. Am. Chem. Soc*. **2016**, *138*, 14783−14788.

S3. Shinde, D. B.; Kandambeth, S.; Pachfule, P.; Kumar, R. R. I.; Banerjee, R. Bifunctional covalent organic frameworks with two dimensional organocatalytic micropores. *Chem. Commun*. **2015**, *51*, 310-313.

S4. Ma, Y.-X.; Li, Z.-J.; Wei, L.; Ding, S.-Y.; Zhang, Y.-B.; Wang, W. A Dynamic Three-Dimensional Covalent Organic Framework. *J. Am. Chem. Soc*. **2017**, *139*, 4995−4998.

S5. Luis-Barrerra, J.; Cano, R.; Imani-Shakibaei, G.; Heras-Domingo, J.; Pérez-Carvajal, J.; Imaz, I.; Maspoch, D.; Solans-Monfort, X.; Alemán, J.; Mas-Ballesté, R. Switching acidic and basic catalysis through supramolecular functionalization in a porous 3D covalent imine-based material. *Catal. Sci. Technol*. **2019**, *9*, 6007-6014.

S6. Ding, L.-G.; Yao, B.-J.; Li, F.; Shi, S.-C.; Huang, N.; Yin, H.-B.; Guan, Q.; Dong, Y.-B. Ionic liquid-decorated COF and its covalent composite aerogel for selective CO_2 adsorption and catalytic conversion. *J. Mater. Chem. A* **2019**, *7*, 4689-4698.

S7. Saptal, V.; Shinde, D. B.; Banerjee, R.; Bhanage, B. M. State-of-the-art catechol porphyrin COF catalyst for chemical fixation of carbon dioxide via cyclic carbonates and oxazolidinones. *Catal. Sci. Technol*. **2016**, *6*, 6152-6158.

S8. Mu, Z.-J. Ding, X.; Chen, Z.-Y.; Han, B.-H. Zwitterionic Covalent Organic Frameworks as Catalysts for Hierarchical Reduction of CO_2 with Amine and Hydrosilane. *ACS Appl. Mater. Interfaces* **2018**, *10*, 41350-41358.

S9. Zhi, Y.; Shao, P.; Feng, X.; Xia, H.; Zhang, Y.; Shi, Z.; Mu, Y.; Liu, X. Covalent organic frameworks: efficient, metal-free, heterogeneous organocatalysts for chemical fixation of CO_2 under mild conditions. *J. Mater. Chem. A* **2018**, *6*, 374-382.

S10. Sun, Q.; Tang, Y.; Aguila, B.; Wang, S.; Xiao, F.-S.; Thallapally, P. K.; Al-Enizi, A. M.; Nafady, A. Ma, S. Reaction Environment Modification in Covalent Organic Frameworks for Catalytic Performance Enhancement. *Angew. Chem. Int. Ed*. **2019**, *131*, 8762-8767.

S11. Peng, Y.; Hu, Z.; Gao, Y.; Yuan, D.; Kang, Z.; Qian, Y.; Yan, N.; Zhao, D. Synthesis of a Sulfonated Two-Dimensional Covalent Organic Framework as an Efficient Solid Acid Catalyst for Biobased Chemical Conversion. *ChemSusChem* **2015**, *8*, 3208–3212.

S12. Gao, W. ; Sun, X.; Niu, H.; Song, X.; Li, K.; Gao, H.; Zhang, W.; Yu, J.; Jia, M. Phosphomolybdic acid functionalized covalent organic frameworks: Structure characterization and catalytic properties in olefin epoxidation. *Microporous Mesoporous Mater*. **2015**, *213*, 59–67.

S13. Xu, H.; Chen, X.; Gao, J.; Lin, J.; Addicoat, M.; Irle, S.; Catalytic covalent organic frameworks via pore surface engineering. Jiang, D. *Chem.Commun*. **2014**, *50*, 1292—1294.

S14. Li, X.; Wang, Z.; Sun, J.; Gao, J.; Zhao, Y.; Cheng, P.; Aguila, B.; Ma, S.; Chen, Y.; Zhang, Z. Squaramide-decorated covalent organic framework as a new platform for biomimetic hydrogen-bonding organocatalysis. *Chem. Commun*. **2019**, *55*, 5423-5426.

S15. Wu, Y.; Xu, H.; Chen, X.; Gao, J.; Jiang, D. A π-electronic covalent organic framework catalyst: π-walls as catalytic beds for Diels–Alder reactions under ambient conditions. *Chem. Commun*. **2015**, *51*, 10096-10098.

S16. Shen, J.-C.; Jiang, W.-L.; Guo, W.-D.; Qi, Q.-Y.; Ma, D.-L.; Lou, X.; Shen, M.; Hu, B.; Yang, H.-B.; Zhao, X. A rings-in-pores net: crown ether-based covalent organic frameworks for phase-transfer catalysis. *Chem. Commun*. **2020**, *56*, 595-598.

S17. Zhang, W.; Jiang, P.; Wang, Y.; Zhang, J.; Gao, Y.; Zhang, P. Bottom-up approach to engineer a molybdenum-doped covalent-organic framework catalyst for selective oxidation reaction. *RSC Adv*. **2014**, *4*, 51544–51547.

S18. Mu, M. ; Wang, Y.; Qin, Y.; Yan, X.; Li, Y.; Chen, L. Two-Dimensional Imine-Linked Covalent Organic Frameworks as a Platform for Selective Oxidation of Olefins. *ACS Appl. Mater. Interfaces* **2017**, *9*, 22856-22863.

S19. Zhao, M.; Wu, C.-D. Synthesis and post-metalation of a covalent-porphyrinic framework for highly efficient aerobic epoxidation of olefins. *Catal. Commun*. **2017**, *99*, 146-149.

S20. Yu, D.; Gao, W.; Xing, S.; Lian, L.; Zhang, H.; Wanga, X.; lou, D. Fe-doped $H_3PMo_{12}O_{40}$ immobilized on covalent organic frameworks (Fe/PMA@COFs): a heterogeneous catalyst for the epoxidation of cyclooctene with H_2O_2. *RSC Adv*. **2019**, *9*, 4884-4891.

S21. Zhang, W.; Jiang, P.; Wang, Y.; Zhang, J.; Zhang, P. Bottom-up approach to engineer two covalent porphyrinic frameworks as effective catalysts for selective oxidation. *Catal. Sci. Technol*. **2015**, *5*, 101 -104.

S22. Chakraborty, D.; Nandi, S.; Mullangi, D.; Haldar, S.; Vinod, C. P.; Vaidhyanathan, R. Cu/Cu_2O Nanoparticles Supported on a Phenol–Pyridyl COF as a Heterogeneous Catalyst for the Synthesis of Unsymmetrical Diynes via Glaser–Hay Coupling. *ACS Appl. Mater. Interfaces* **2019**, *11*, 15670–15679.

S23. Han, Y.; Zhang, M.; Zhang, Y.-Q.; Zhang, Z.-H. Copper immobilized at a covalent organic framework: an efficient and recyclable heterogeneous catalyst for the Chan–Lam coupling reaction of aryl boronic acids and amines. *Green Chem*. **2018**, *20*, 4891-4900.

S24. Vardhan, H.; Verma, G.; Ramani, S.; Nafady, A.; Al-Enizi, A. M.; Pan, Y.; Yang, Z.; Yang, H.; Ma, S. Covalent Organic Framework Decorated with Vanadium as a New Platform for Prins Reaction and Sulfide Oxidation. *ACS Appl. Mater. Interfaces* **2019**, *11*, 3070-3079.

S25. Vardhan, H.; Hou, L.; Yee, E.; Nafady, A.; Al-Abdrabalnabi, M. A.; Al-Enizi, A. M.; Pan, Y.; Yang, Z.; Ma, S. Vanadium Docked Covalent-Organic Frameworks: An Effective Heterogeneous Catalyst for Modified Mannich-Type Reaction. *ACS Sustainable Chem. Eng*. **2019**, *7*, 4878-4888.

S26. Cifuentes, J. M. C.; Ferreira, B. X.; Esteves, P. M.; Buarque, C. D. Decarboxylative Cross-Coupling of Cinnamic Acids Catalyzed by Iron-Based Covalent Organic Frameworks. *Topics in Catalysis* **2018**, *61*, 689-698.

S27. Maia, R. A.; Berg, F.; Ritleng, V.; Louis, B.; Esteves, P. M. Design, Synthesis and Characterization of Nickel-Functionalized Covalent Organic Framework NiCl@RIO-12 for Heterogeneous Suzuki-Miyaura Catalysis. *Chem. Eur. J*. **2020**, *26*, 2051-2059.

S28. Haug, W. K.; Wolfson, E. R.; Morman, B. T.; Thomas, C. M.; McGrier, P. L. A Nickel-Doped Dehydrobenzoannulene-Based Two-Dimensional Covalent Organic Framework for the Reductive Cleavage of Inert Aryl C–S Bonds. *J. Am. Chem. Soc*. **2020**, *142*, 5521-5525.

S29. Mullangi, D.; Chakraborty, D.; Pradeep, A.; Koshti, V.; Vinod, C. P.; Panja, S.; Nair, S.; Vaidhyanathan, R. Highly Stable COF-Supported Co/$Co(OH)_2$ Nanoparticles Heterogeneous Catalyst for Reduction of Nitrile/Nitro Compounds under Mild Conditions. *Small* **2018**, *14*, 1801233.

S30. Ma, Y.; Liu, X.; Guan, X.; Li, H.; Yusran, Y.; Xue, M.; Fang, Q.; Yan, Y.; Qiua, S.; Valtchev, V. One-pot cascade syntheses of microporous and mesoporous pyrazine-linked covalent organic frameworks as Lewis-acid catalysts. *Dalton Trans*. **2019**, *48*, 7352-7357.

S31. Sun, Q.; Aguila, B.; Ma, S. A bifunctional covalent organic framework as an efficient platform for cascade catalysis. *Mater. Chem. Front*. **2017**, *1*, 1310-1316.

S32. Leng, W.; Peng, Y.; Zhang, J.; Lu, H.; Feng, X.; Ge, R.; Dong, B.; Wang, B.; Hu, X.; Gao, Y. Sophisticated Design of Covalent Organic Frameworks with Controllable Bimetallic Docking for a Cascade Reaction. *Chem. Eur. J*. **2016**, *22*, 9087 – 9091.

S33. Bhadra, M.; Sasmal, H. S.; Basu, A.; Midya, S. P.; Kandambeth, S.; Pachfule, P.; Balaraman, E.; Banerjee, R. Predesigned Metal-Anchored Building Block for In Situ Generation of Pd Nanoparticles in Porous Covalent Organic Framework: Application in Heterogeneous Tandem Catalysis. *ACS Appl. Mater. Interfaces* **2017**, *9*, 13785−13792.

S34. Lu, S.; Hu, Y.; Wan, S.; McCaffrey, R.; Jin, Y.; Gu, H.; Zhang, W. Synthesis of Ultrafine and Highly Dispersed Metal Nanoparticles Confined in a Thioether-Containing Covalent Organic Framework and Their Catalytic Applications. *J. Am. Chem. Soc*. **2017**, *139*, 47, 17082-17088.

S35. Shi, X.; Yao, Y.; Xu, Y.; Liu, K.; G.; Chi, L.; Lu, G. Imparting Catalytic Activity to a Covalent Organic Framework Material by Nanoparticle Encapsulation. *ACS appl. Mater. Interfaces* **2017**, *9*, 7481-7488.

S36. Pachfule, P.; Kandambeth, S.; Díaz, D. D.; Banerjee, R. Highly stable covalent organic framework–Au nanoparticles hybrids for enhanced activity for nitrophenol reduction. *Chem. Commun*. **2014**, *50*, 3169—3172.

S37. Wan, X.; Wang, X.; Chen, G.; Guo, C.; Zhang, B. Covalent organic framework/nanofibrillated cellulose composite membrane loaded with Pd nanoparticles for dechlorination of dichlorobenzene. *Mater. Chem. Phys*. **2020**, *246*, 122574.

S38. Tan, X.; Zeng, W.; Fan, Y.; Yan, J.; Zhao, G. Covalent organic frameworks bearing pillar[6]arene-reduced Au nanoparticles for the catalytic reduction of nitroaromatics. *Nanotechnology* **2020**, *31*, 135705.

S39. Li, X.; Zhang, C.; Luo, M.; Yao, Q.; Lu, Z.-H. Ultrafine Rh nanoparticles confined by nitrogen-rich covalent organic frameworks for methanolysis of ammonia borane. *Inorg. Chem. Front*. **2020**, *7*, 1298-1306.

S40. Tao, R.; Shen, X.; Hu, Y.; Kang, K.; Zheng, Y.; Luo, S.; Yang, S.; Li, W.; Lu, S.; Jin, Y.; Qiu, L.; Zhang, W. Phosphine-Based Covalent Organic Framework for the Controlled Synthesis of Broad-Scope Ultrafine Nanoparticles. *Small* **2020**, *16*, 1906005.

S41. Gonçalves, L. P. L.; Christensen, D. B.; Meledina, M.; Salonen, L. M.; Petrovykh, D. Y.; Carbó-Argibay, E.; Sousa, J. P. S.; Soares, O. S. G. P.; Pereira, M. F. R.; Kegnæs, S.; Kolen'ko, Y. V. Selective formic acid dehydrogenation at low temperature over a RuO_2/COF pre-catalyst synthesized on the gram scale. *Catal. Sci. Technol*. **2020**, *10*, 1991-1995.

S42. Zhang, Q.-P.; Sun, Y.-l.; Cheng, G.; Wang, Z.; Ma, H.; Ding, S.-Y.; Tan, B.; Bu, J.-h.; Zhang, C. Highly dispersed gold nanoparticles anchoring on post-modified covalent organic framework for catalytic application. *Chem. Eng. J*. **2019**, *391* 123471.

S43. Gong, W.; Wu, Q.; Jiang, G.; Li, G. Ultrafine silver nanoparticles supported on a covalent carbazole framework as high-efficiency nanocatalysts for nitrophenol reduction. *J. Mater. Chem. A* **2019**, *7*, 13449–13454.

S44. Ding, Z.-D.; Wang, Y.-X.; Xi, S.-F.; Li, Y.; Li, Z.; Ren, X.; Gu, Z.-G. A Hexagonal Covalent Porphyrin Framework as an Efficient Support for Gold Nanoparticles toward Catalytic Reduction of 4-Nitrophenol. *Chem. Eur. J*. **2016**, *22*, 17029-17036.

S45. GonÅalves, R. S. B.; de Oliveira, A. B. V.; Sindra, H. C.; Archanjo, B. S.; Mendoza, M. E.; Carneiro, L. S. A.; Buarque, C. D.; Esteves, P. M. Heterogeneous Catalysis by Covalent Organic Frameworks (COF): $Pd(OAc)_2$@COF-300 in Cross-Coupling Reaction. *ChemCatChem* **2016**, *8*,743–750.

S46. Kaleeswaran, D.; Antony, R.; Sharma, A.; Malani, A.; Murugavel, R. Catalysis and CO_2 Capture by Palladium-Incorporated Covalent Organic Frameworks. *ChemPlusChem* **2017**, *82*, 1253–1265.

S47. Zhu, W.; Wang, X.; Li, T.; Shen R.; Hao, S.-J.; Li, Y.; Wang, Q.; Li, Z.; Gu, Z.-G. Porphyrin-based porous polyimide polymer/Pd nanoparticle composites as efficient catalysts for Suzuki–Miyaura coupling reactions. *Polym. Chem.* **2018**, *9*, 1430 –1438.

S48. Ding, S.-Y.; Gao, J.; Wang, Q.; Zhang, Y.; Song, W.-G.; Su, C.-Y.; Wang, W. Construction of Covalent Organic Framework for Catalysis: Pd/COF-LZU1 in Suzuki–Miyaura Coupling Reaction. *J. Am. Chem. Soc*. **2011**, *133*, 19816–19822.

S49. Hou, Y.; Zhang, X.; Sun, J.; Lin, S.; Qi, D.; Hong, R.; Li, D.; Xiao, X.; Jiang, J. Good Suzuki-coupling reaction performance of Pd immobilized at the metal-free porphyrin-based covalent organic framework. *Microporous Mesoporous Mater.* **2015**, *214*, 108–114.

S50. Wang, J.-C.; Liu, C.-X.; Kan, X.; Wu, X.-W.; Kan, J.-L.; Dong, Y.-B. Pd@COF-QA: a phase transfer composite catalyst for aqueous Suzuki–Miyaura coupling reaction. *Green Chem*. **2020**, *22*, 1150-1155.

S51. Yang, J.; Wu, Y.; Wu, X.; Liu, W.; Wang, Y.; Wang, J. An N-heterocyclic carbene-functionalised covalent organic framework with atomically dispersed palladium for coupling reactions under mild conditions. *Green Chem*. **2019**, *21*, 5267-5273.

S52. Sadhasivam, V.; Balasaravanan, R.; Chithiraikumar, C.; Siva, A. Incorporating $Pd(OAc)_2$ on Imine Functionalized Microporous Covalent Organic Frameworks: A Stable and Efficient Heterogeneous Catalyst for Suzuki-Miyaura Coupling in Aqueous Medium. *Chem. Select* **2017**, *2*, 1063–1070.

S53. Pachfule, P.; Panda, M. K.; Kandambeth, S.; Shivaprasad, S. M.; Díaz, D. D.; Banerjee, R. Multifunctional and robust covalent organic framework–nanoparticle hybrids. *J. Mater. Chem. A* **2014**, *2*, 7944–7952.

S54. Leng, W.; Ge, R.; Dong, B.; Wang, C.; Gao, Y. Bimetallic docked covalent organic frameworks with high catalytic performance towards tandem reactions. *RSC Adv*. **2016**, *6*, 37403 –37406.

S55. Han, J.; Sun, X.; Wang, X.; Wang, Q.; Hou, S.; Song, X.; Wei, Y.; Wang, R.; Ji, W. Covalent Organic Framework as a Heterogeneous Ligand for the Regioselective Oxidative Heck Reaction. *Org. Lett*. **2020**, *22*, 1480-1484.

S56. Mullangi, D.; Nandi, S.; Shalini, S.; Sreedhala, S.; Vinod, C. P.; Vaidhyanathan, R. Pd loaded amphiphilic COF as catalyst for multi-fold Heck reactions, C-C couplings and CO oxidation. *Sci. rep*. **2015**, *5*, 10876.

S57. Guana, P.; Qiua, J.; Zhaoa, Y.; Wang, H.; Lia, Z.; Shib, Y.; Wang, J. A novel crystalline azine-linked three-dimensional covalent organic framework for CO_2 capture and conversion. *Chem. Commun*. **2019**, *55*, 12459-12462.

S58. Chakraborty, D.; Shekhar, P.; Singh, H. D.; Kushwaha, R.; Vinod, C. P.; Vaidhyanathan, R. Ag Nanoparticles Supported on a Resorcinol-Phenylenediamine-Based Covalent Organic Framework for Chemical Fixation of CO_2. *Chem. Asian J*. **2019**, *14*, 4767-4773.

S59. Lin, S.; Hou, Y.; Deng, X.; Wang, H.; Suna, S.; Zhang, X. A triazine-based covalent organic framework/palladium hybrid for one-pot silicon-based cross-coupling of silanes and aryl iodides. *RSC Adv*. **2015**, *5*, 41017-41024.

S60. Chen, G.-J.; Li, X.-B.; Zhao, C.-C.; Ma, H.-C.; Kan, J.-L.; Xin, Y.-B.; Chen, C.-X.; Dong, Y.-B. Ru Nanoparticles-Loaded Covalent Organic Framework for Solvent-Free One-Pot Tandem Reactions in Air. *Inorg. Chem*. **2018**, *57*, 2678−2685.

S61. Pan, S.; Yao, D.; Liang, A.; Wen, G.; Jiang, Z. New Ag-Doped COF Catalytic Amplification Aptamer Analytical Platform for Trace Small Molecules with the Resonance Rayleigh Scattering Technique. *ACS Appl. Mater. Interfaces* **2020**, *12*, 12120-12132.

S62. Heintz, P. M.; Schumacher, B. P.; Chen, M.; Huang, W.; Stanley, L. M. A Pd(II)-Functionalized Covalent Organic Framework for Catalytic Conjugate Additions of Arylboronic Acids to β,β-Disubstituted Enones. *ChemCatChem* **2019**, *11*, 4286-4290.

S63. Vardhan, H.; Pan, Y.; Yang, Z.; Verma, G.; Nafady, A.; Al-Enizi, A. M.; Alotaibi, T. M.; Almaghrabi, O. A.; Ma, S. Iridium complex immobilization on covalent organic framework for effective C—H borylation. *APL Mater*. **2019**, *7*, 101111.

S64. Hausoul, P. J. C.; Eggenhuisen, T. M.; Nand, D.; Baldus, M.; Weckhuysen, B. M.; Gebbink, R. J. M. K.; Bruijnincx, P. C. A. Development of a 4,4′-biphenyl/phosphine-based COF for the heterogeneous Pd-catalysed telomerisation of 1,3-butadiene. *Catal. Sci. Technol*. **2013**, *3*, 2571-2579.